Suppression of epithelial proliferation and tumourigenesis by immunoglobulin A

Gregory P. Donaldson[1*], Gabriella L. Reis[1], Marwa Saad[1], Christopher Wichmann[1,2], Izabela Mamede [1], Guo Chen[1], Nicole L. DelGaudio[1], Dayu Zhang[3], Begüm Aydin[1], Caroline E. Harrer[1], Tiago B.R. Castro[2], Sergei Grivennikov[4], Bernardo S. Reis[1], Beth M. Stadtmueller[3,5,6], Gabriel D. Victora[2,7], and Daniel Mucida[1,7*]

[1]Laboratory of Mucosal Immunology, The Rockefeller University, New York, United States
[2]Laboratory of Lymphocyte Dynamics, The Rockefeller University, New York, United States
[3]Department of Biochemistry, University of Illinois, Urbana, United States
[4]Departments of Medicine and Biomedical Sciences, Cedars-Sinai Cancer, Cedars-Sinai Medical Center, Los Angeles, United States
[5]Carl R. Woese Institute for Genomic Biology, University of Illinois, Urbana, USA
[6]Department of Biomedical and Translational Sciences, Carle Illinois College of Medicine, University of Illinois, Urbana, USA
[7]Howard Hughes Medical Institute, The Rockefeller University, New York, United States

*Materials & Correspondence: gdonaldson@rockefeller.edu (G.P.D.) or mucida@rockefeller.edu (D.M.)

Immunoglobulin A (IgA) is the most abundant antibody isotype produced across mammals and plays a specialized role in mucosal homeostasis[1]. Constantly secreted into the lumen of the intestine, IgA binds commensal microbiota to regulate their colonization and function[2,3] with unclear implications for health. IgA deficiency is common in humans but is difficult to study due to its complex aetiology and comorbidities[4–8]. Using genetically and environmentally controlled mice, here we show that IgA-deficient animals have increased susceptibility to endogenous colorectal tumours. Cellular and molecular analyses revealed that, in the absence of IgA, colonic epithelial cells induce antibacterial factors and accelerate cell cycling in response to the microbiota. Oral treatment with IgA was sufficient to both reduce steady-state proliferation and protect mice from tumours, but this function was due to antibody structure rather than binding specificity. In both organoid and monolayer culture systems, IgA directly suppressed epithelial growth. Co-immunoprecipitation mass spectrometry and a targeted CRISPR screen identified DMBT1 as an IgA-binding epithelial surface protein required for IgA-mediated suppression of proliferation. Together, IgA and DMBT1 regulate Notch signalling and tune the normal cycling of absorptive colonocyte progenitors. In mice, deleting the transmembrane and cytoplasmic signalling portions of DMBT1 or blocking Notch signalling was sufficient to reverse both the increased proliferation and tumour susceptibility of IgA knockouts. These experiments establish a homeostatic function for IgA in tempering physiological epithelial responses to microbiota to maintain mucosal health.

44 In the absence of infection or disease, IgA is constantly produced in the intestine, where it is
45 secreted into the lumen in the form of secretory IgA (SIgA) and binds commensal microbiota[9]. In
46 humans, selective IgA deficiency is the most common primary immunodeficiency, clinically
47 defined as low (<7 mg/dL) serum IgA levels with normal levels of IgM and IgG[10]. These patients
48 have an increased risk of respiratory/gastrointestinal infections, inflammatory/autoimmune
49 disorders[10], and gastrointestinal cancers[11]. IgA is known to control mucosal pathogens[12–14];
50 however, the impact of IgA on inflammatory diseases and malignancy remains unclear. Recent
51 studies have indicated that IgA deficiency is associated with changes in the microbiota and
52 systemic inflammation[4,6,7,15], which may be more pronounced in patients with undetectable IgA[8]. A
53 compensatory increase in the other major secreted antibody isotype, IgM, is insufficient to rescue
54 these effects[4]. The association with malignancy, first observed clinically decades ago[16,17], may be
55 related to the influence of specific species of gut microbiota on colon cancer[18–20]. The largest study
56 on IgA deficiency (2,495 patients matched to 24,509 controls) showed double all-cause mortality
57 and an increased risk of colon and prostate cancers[21]. An inverse analysis of patients with
58 gastrointestinal cancer found an increased frequency of IgA deficiency[22]. Among patients with
59 combined variable immunodeficiency, those with colon cancer were more likely to have a
60 deficiency in IgA[23]. Despite these associations, the polygenic nature of IgA deficiency, clinical
61 criteria based on an arbitrary cutoff for serum (not mucosal) concentration, and various
62 comorbidities thwart the attribution of these health effects to isotype-specific functions.
63
64 Most known functions of intestinal IgA have been discovered using mouse models, showing that
65 these antibodies prevent mucosal infections[12–14] and affect the form and function of the gut
66 microbiome[24–31]. IgA can be polyreactive[32,33], cross-reactive[34,35], or species-specific[36], allowing
67 binding to a substantial fraction of the mammalian microbiota at the cellular level. The effects on
68 bacteria can vary; IgA controls *Bacteroides thetaiotaomicron* gene expression[37,38], *Salmonella*
69 *enterica* swimming motility[14], *Bacteroides fragilis* mucosal anchoring[39], and *Escherichia coli*
70 surface receptor activities[40]. However, beyond limiting invasive pathogenesis, mechanisms
71 connecting microbiota-IgA interactions to health and disease are lacking. An isotype-specific
72 knockout mouse model (*Igha*$^{-/-}$, hereafter referred to as IgA$^{-/-}$) causing total IgA deficiency was
73 established more than 20 years ago[41]. This mutation causes an increase in serum and mucosal
74 IgM[41], which is often observed in human IgA deficiency[4]. IgA$^{-/-}$ mice have a few described
75 phenotypes[13] and are largely indistinguishable from wild-type controls in a dextran sodium
76 sulfate colitis model[42], suggesting that IgA is dispensable for the normal intestinal barrier. In
77 contrast, polymeric immunoglobulin receptor (pIgR) knockouts, which are unable to actively

transport antibodies to the lumen of the intestine, are more susceptible to colitis[42], highlighting the importance of compensatory IgM or other functions of pIgR in supporting the barrier. pIgR binds dimeric IgA or pentameric IgM and directs their transcytosis to the apical surface, where proteases cleave the receptor to release the antibody into the lumen. The antibody-binding ectodomain of pIgR, known as the secretory component, is secreted even in the absence of IgA and may have independent functions[43,44]. While many secreted host factors interact with bacteria to reinforce the epithelial barrier, IgA may have more nuanced roles, as reflected in the perplexing epidemiology of human IgA deficiency.

Impact of IgA deficiency during steady state and cancer models

To study the direct physiological consequences of IgA deficiency and the fundamental isotype-specific functions of IgA in the gut, female $IgA^{+/-}$ mice were bred with $IgA^{-/-}$ males to control for the effects of maternal milk IgA on normal immune development[45]. $IgA^{+/-}$ mice had comparable levels of faecal IgA to $IgA^{+/+}$ littermates (**Extended Data Fig. 1a-b**), indicating that heterozygotes can serve as a normal control. Co-housed littermates were used in all experiments to minimize environmental variables and normalize the microbiome through both vertical and horizontal transmission[46]. For an unbiased analysis of possible IgA effects on the region of the gut with the highest concentration of gut bacteria[47], mid-colon tissues were sampled at steady state for bulk RNA-Seq (**Fig. 1a**). Overall, the number of differentially expressed genes was modest and there was no evidence of overt inflammation in the $IgA^{-/-}$ colon. Nevertheless, $IgA^{-/-}$ mice showed alterations in many epithelial-related genes, including a decrease in goblet cell markers (*Spink4*, *Fcgbp*, *Capn9,* and *Tff3*) and other cell type-specific markers such as *SpiB* (M cell transcription factor) and *Rgs4* (enteroendocrine cell marker) (**Fig. 1a, Supplementary Table 1**). This coincided with an increase in *Nox1*, a specific marker for the highly proliferative transit-amplifying cells[48], with concordant increases in general cell cycling-related pathways and specific genes (*Mcc* and *Sass6*) (**Fig. 1a**). These results point to a physiological role for IgA in balancing proliferation and differentiation in the intestinal epithelium in steady state conditions.

Next, we used a murine model of endogenous colon cancer as a perturbation to test for further effects of IgA revealed by the disease state. $IgA^{-/-}$ mice were crossed with a strain harbouring a *Cdx2* promoter-driven, tamoxifen-inducible Cre recombinase and loxP-flanked alleles of the tumour suppressor *APC*, which is mutated in more than 90% of human colorectal tumours[49,50]. This allows for temporally controlled homozygous knockout of *APC* in a fraction of colonic epithelial cells (**Fig. 1b**). To compare the steady-state transcriptome changes observed in $IgA^{-/-}$

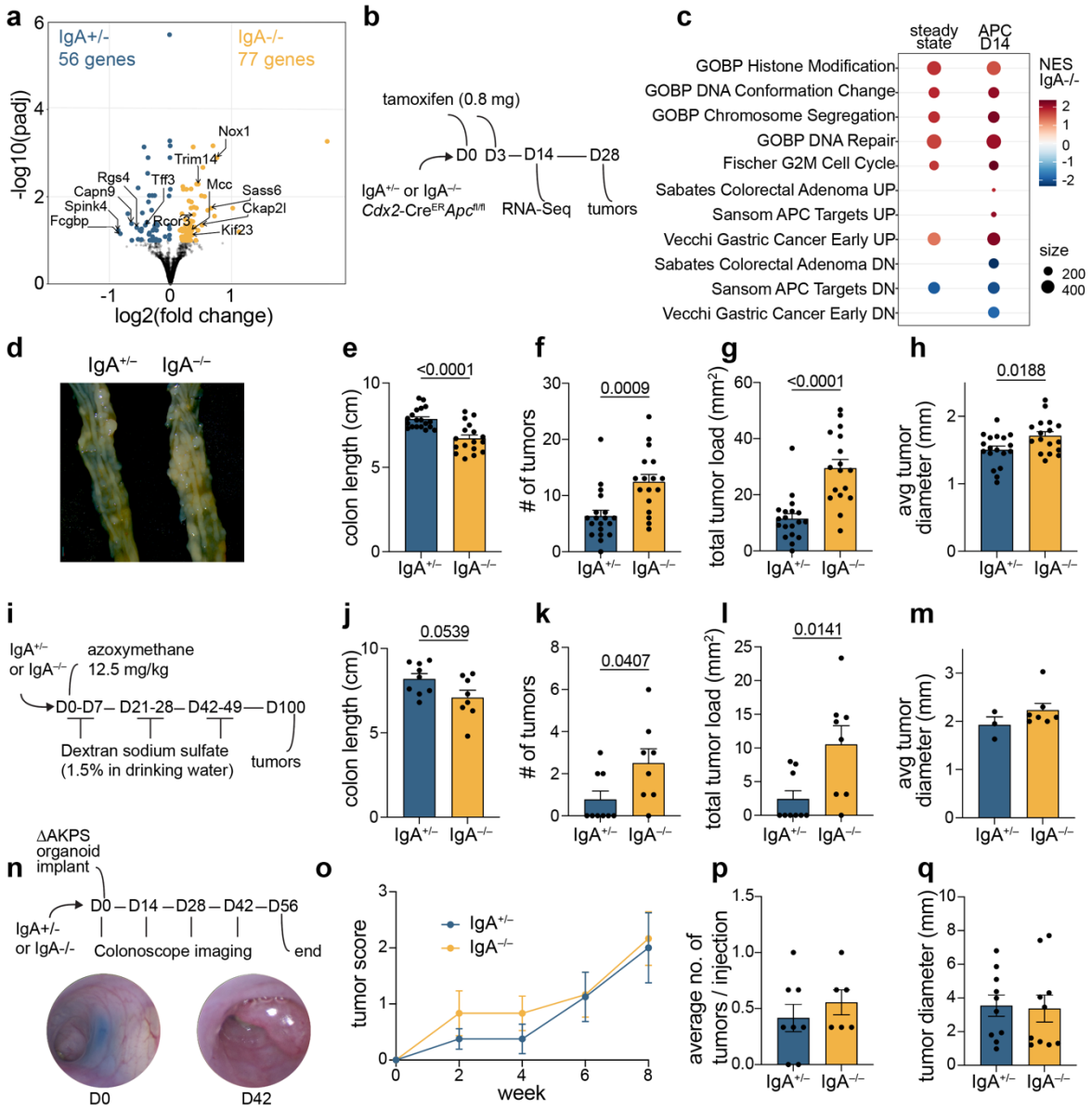

Fig. 1 | IgA$^{-/-}$ mice have pro-tumour alterations to colon tissue and increased susceptibility to endogenous colorectal cancer models. a, Bulk RNA-Seq of colon tissue from IgA$^{+/-}$ and IgA$^{-/-}$ mice during steady state revealed upregulation of transit-amplifying cell markers and downregulation of goblet cell markers (n = 5). **b**, Experimental design for studies of IgA in the context of epithelial-specific loss of *APC*. **c**, Gene set enrichment analyses indicated a pro-cancerous phenotype of IgA$^{-/-}$ mice that was exacerbated after APC loss (n = 5 steady, 4 APC, visible dots only for gene sets where adjusted $p < 0.05$). **d-h**, On day 28, mice were sacrificed and assessed for colon length, number of colon tumours, total tumour load, and average tumour size (pooled, 4 cohorts, n = 19, 17). **i**, Experimental design for azoxymethane (AOM) and dextran sodium sulfate (DSS) model of colorectal cancer. **j-m**, Mice were sacrificed at day 100 to assess tumour outcomes as in **e-h** (pooled 2 cohorts, n = 9, 8 except panel m includes only mice with tumours: n = 3, 7). **n**, Experimental design and example images for colonoscope-guided implant of quadruple-knockout (*APC*, *Kras*, *P53*, *Smad4*) organoid cells. **o**, Tumour growth was tracked longitudinally by colonoscope and scored based on the size of the tumour relative to the colon circumference (pooled 2 cohorts, n = 8, 6, details in methods). **p**, After 8 weeks, mice were sacrificed to assess the average number of tumours per injection (not all injections result in implantation) and **q**, tumour size (n = 10). (t-tests, p values hidden when $p > 0.1$)

131 colon samples, we harvested tissue for the same analysis at an early, pre-tumour time point (**Fig.**
132 **1b-c**). Despite the synchronized loss of APC in these co-housed littermates, there were substantial
133 (hundreds of genes) differences in gene expression patterns between IgA$^{+/-}$ and IgA$^{-/-}$ animals
134 (**Extended Data Fig. 1c, Supplementary Table 2**). Specifically, pathways related to epithelial cell
135 proliferation, APC mutation, and human colorectal cancer were enhanced in IgA$^{-/-}$ mice (**Fig. 1c**).
136 At the pathway level, modest alterations at steady state in IgA$^{-/-}$ mice mirrored the more dramatic
137 phenotype induced by the APC mutation (**Fig. 1c**). Analysis of the specific genes altered during
138 steady state showed that most of these IgA-modulated genes were also modulated by *APC* loss,
139 with nearly perfect directional concordance between IgA deficiency and *APC* loss (**Extended Data**
140 **Fig. 1d**). These molecular results were predictive of gross morphological outcomes (**Fig. 1d**).
141 While IgA$^{+/+}$ and IgA$^{+/-}$ mice were indistinguishable (**Extended Data Fig. 1e**), IgA$^{-/-}$ mice had
142 shortened colons (**Fig. 1e**), increased number of tumours (**Fig. 1f**), and increased total tumour
143 load (**Fig. 1g**) when compared to cohoused IgA$^{+/-}$ littermates. The size of the tumours appeared to
144 slightly increase (**Fig. 1h**), but the effect size on the number of tumours was much more
145 substantial. Though this model is dependent on inflammation-driven tumour growth[49,50], faecal
146 lipocalin as a measure of inflammation (**Extended Data Fig. 1f**), and expression levels of
147 cytokines in bulk RNA-Seq (**Extended Data Fig. 1g**) showed no differences in IgA$^{-/-}$ mice,
148 suggesting that the impact of IgA was not related to general increases in inflammatory signals.
149 These molecular and tumour analyses indicate that IgA$^{-/-}$ mice are more susceptible to
150 endogenous colorectal cancer. This effect may be due to alterations in the steady state that
151 promote tumourigenesis.
152
153 To expand on these findings, IgA$^{+/-}$ and IgA$^{-/-}$ mice were subjected to an independent colorectal
154 cancer model in which injection of the mutagen azoxymethane is followed by three rounds of
155 exposure to dextran sodium sulfate (AOM-DSS) in their drinking water (**Fig. 1i**), mimicking colitis-
156 associated CRC[50]. IgA$^{-/-}$ mice had similar colon length (**Fig. 1j**) but showed more tumours (**Fig.**
157 **1k**) and higher overall tumour load (**Fig. 1l**) than IgA$^{+/-}$ controls. As previously reported[42], IgA$^{-/-}$
158 mice were slightly more susceptible to DSS-induced weight loss (**Extended Data Fig. 1h**). While
159 most IgA$^{-/-}$ mice developed tumours even when exposed to a relatively low dose of DSS (1.5%), a
160 minority of IgA$^{+/-}$ mice developed tumours (**Extended Data Fig. 1i**). The average tumour size was
161 comparable among the tumour-bearing animals (**Fig. 1m**). These results are consistent with the
162 APC-driven model, suggesting a specific role for IgA in tumourigenesis, but not growth. To directly
163 test whether IgA affects tumour growth, IgA$^{+/-}$ and IgA$^{-/-}$ mice were subjected to a model that
164 bypasses the transformation stage. Mouse colon organoids with four cancer-related gene

mutations (*APC*, *Kras*, *P53*, *Smad4*) were dissociated into single cells, injected by colonoscope directly into the colon wall, and monitored every two weeks by colonoscopy (**Fig. 1n**). These implanted tumours grew at a similar rate (**Fig. 1o**), with a similar implantation success frequency (**Fig. 1p**), and were similar in size at the endpoint (**Fig. 1q**). Overall, our data indicate that IgA has no apparent role in controlling tumour progression but does actively regulate tumourigenesis in the colon.

The role of IgA-bacteria interactions on tumour susceptibility

As the primary function of IgA at steady state is to regulate the composition and function of the microbiota, we investigated whether IgA$^{-/-}$ mice harbour a pro-tumour microbiome despite being cohoused with littermates. The role of bacteria was first assessed by treating mice with a cocktail of broad-spectrum antibiotics (ampicillin, vancomycin, metronidazole, and neomycin) throughout the experiment (**Fig. 2a**). This treatment reduced tumour numbers in all mice, as previously reported in this model[49], but also prevented the heightened tumour phenotype observed in the untreated IgA$^{-/-}$ mice (**Fig. 2b**). To profile the bacterial microbiome and identify IgA-dependent changes that might explain the observations in Fig. 1, 16S rRNA amplicon sequencing was performed in healthy mice at steady state and two weeks after *APC* deletion. IgA$^{-/-}$ mice were indistinguishable from littermate controls when co-housed throughout the experiment (**Fig. 2c, Extended Data Fig. 2a**). *APC* loss caused a shift in the microbiome, with a loss of diversity, including the depletion of species within the common mouse commensal family *Muribaculaceae* (**Fig. 2c**). This coincided with the outgrowth of *Shigella* and *Helicobacter* species (**Fig. 2c**), both of which have been implicated in colorectal cancer[18–20]. During this dramatic change, IgA still had no apparent influence on the cohoused conditions of these experiments (**Fig. 2c, Extended Data Fig. 2a**). As some IgA-mediated alterations have previously been shown to be mucus-specific[26,39], colon mucus was sampled aseptically for microbiome profiling. This analysis successfully resolved the spatial differences in lumen and mucosal community compositions (**Extended Data Fig. 2a-b**)[47] and revealed that some commensal mucosal species of *Akkermansia* and *Bacteroides* were resilient to *APC* loss (**Extended Data Fig. 2b**). However, even in mucus, no differences were apparent between IgA$^{+/-}$ and IgA$^{-/-}$ samples (**Extended Data Fig. 2a-b**). A statistical test for differential abundance of amplicon sequence variants in microbial communities (ANCOM)[51] revealed no differences between IgA genotypes in the colon lumen or mucus, at steady state, or in the context of *APC* loss (**Extended Data Fig. 2c**). To further test whether the regulation of specific bacterial species is responsible for the effect of IgA on tumour susceptibility, IgA$^{+/-}$ and IgA$^{-/-}$ *Cdx2*^{CreER}*APC*$^{fl/fl}$ mice were c-section re-derived in germ-free isolators, bred to generate littermate

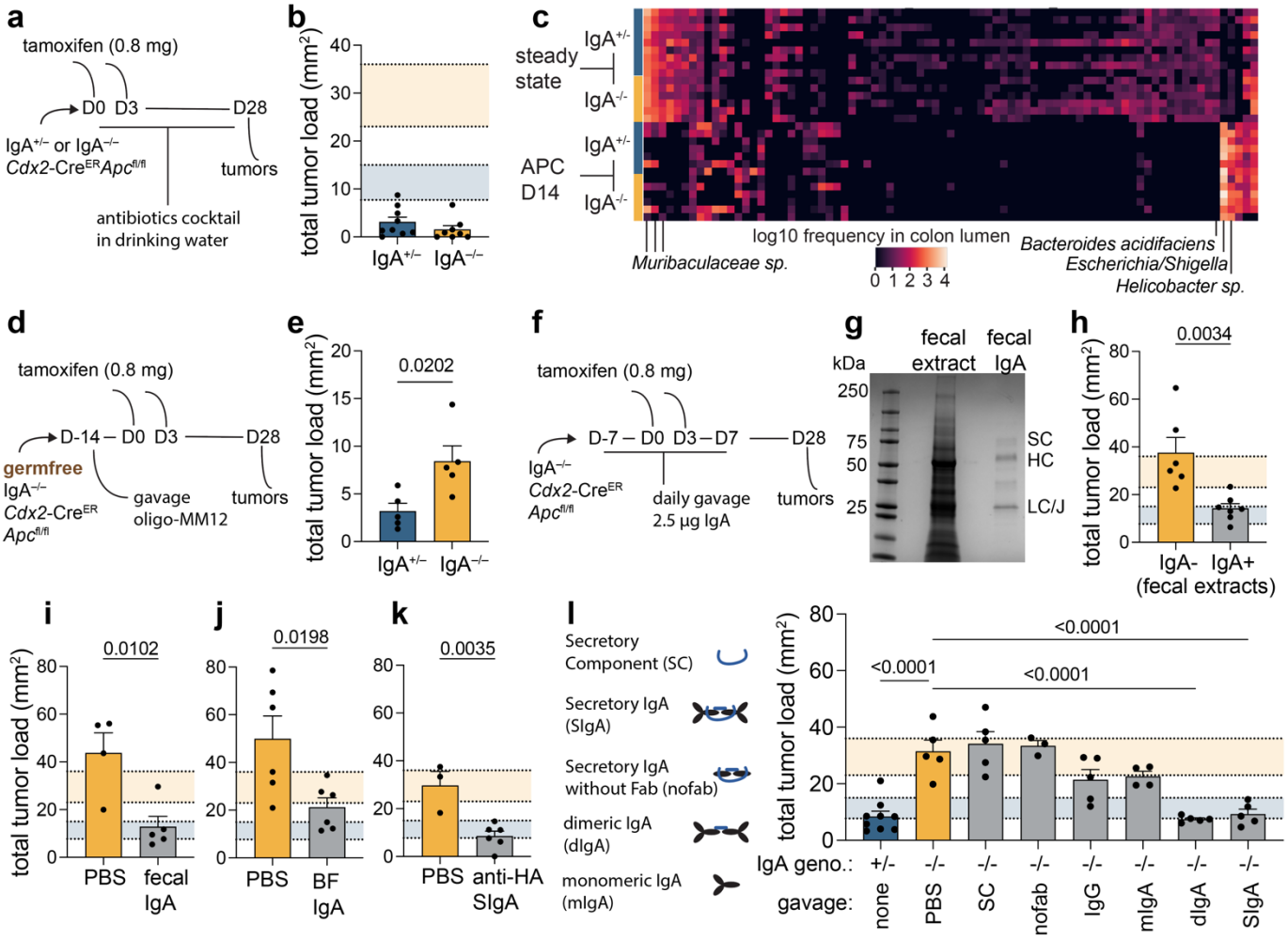

Fig. 2 | Role of the microbiome and IgA structure in tumourigenesis. a, Experimental design for broad spectrum antibiotic treatment (ampicillin, vancomycin, neomycin, metronidazole) to assess the role of microbiome in tumour development in the context of IgA deficiency and *APC* loss. **b**, Total tumour load was dramatically reduced by antibiotic treatment in both IgA$^{+/-}$ and IgA$^{-/-}$ mice to similar levels (pooled 2 cohorts, n = 9, 8). **c**, Heatmap of amplicon sequence variants (columns) identified in colon lumen samples from indicated mice (rows) demonstrates dramatic shift caused by *APC* loss, but no effect of IgA (pooled 2 cohorts, n = 9, 6, 7, 6). **d**, Experimental design for gnotobiotic colon cancer model with a defined microbial community (oligo-MM12)[52] and **e**, corresponding tumour load. **f**, Experimental design for gavage treatments to prevent tumourigenesis in IgA$^{-/-}$ mice in the context of *APC* loss. **g**, Denaturing gel of sterile faecal extract and resulting purified faecal IgA. **h-k**, Total tumour load following *APC* loss in IgA$^{-/-}$ mice treated with **h**, indicated sterile faecal extracts from healthy donor mice (pooled 2 cohorts, n = 6), **i**, purified faecal IgA from healthy donor mice (pooled two cohorts, n = 4, 5), **j**, purified faecal IgA from germfree mice mono-colonized with *Bacteroides fragilis* (pooled two cohorts, n = 6), **k**, recombinant CR9114 anti-influenza HA SIgA (n = 3, 6), or **l**, structural variants of recombinant antibody (n = 9, 5, 5, 3, 5, 4, 5, 5). (Shaded areas in tumour load plots represent the 95% confidence interval of tumour load for IgA$^{+/-}$, blue, and IgA$^{-/-}$, yellow, mice from Fig. 1, t-tests or one-way ANOVA, p values hidden when p > 0.1)

220 controls that all received maternal IgA (**Extended Data Fig. 1b**), and acutely colonized with a
221 twelve species defined gut microbiome[52] prior to inducing *APC* loss (**Fig. 2d**). Although all mice
222 developed fewer tumours with this defined microbiome compared to SPF mice, IgA$^{-/-}$ littermates
223 still developed comparatively more tumours (**Fig. 2e**). Collectively, these experiments involving
224 both measurement and manipulation of the microbiome are consistent with IgA acting on a
225 pathway that is dependent on bacterial colonization but does not relate to the control of particular
226 pro- or anti-tumour species.
227
228 To begin to dissect the mechanism by which IgA prevents tumourigenesis, sufficiency experiments
229 were performed to rescue IgA$^{-/-}$ mice by oral treatment (**Fig. 2f**). First, sterile-filtered faecal
230 extracts (containing proteins and soluble metabolites, **Fig. 2g**) from healthy mice were used for
231 daily oral gavage starting prior to the induction of *APC* loss. Although treatment was ceased 3
232 weeks prior to measuring tumours, extracts from IgA$^{+/-}$ but not IgA$^{-/-}$ mice were sufficient to
233 reduce the tumour load in IgA$^{-/-}$ recipients (**Fig. 2h**). To test whether this impact is conferred by
234 the antibodies or other components of the extract, secretory IgA was purified from the faeces of
235 healthy mice (**Fig. 2g**) and gavaged daily in the same timeframe. The polyclonal IgA preparation
236 from healthy mouse faeces was also sufficient to protect IgA$^{-/-}$ mice from increased tumours (**Fig.
237 2i**). This IgA oral treatment model allowed for the manipulation of antigen specificity, first by
238 purifying IgA from the faeces of germ-free Swiss Webster mice mono-colonized with the model
239 commensal species *Bacteroides fragilis*. Despite the restricted mucosal antigen exposure under
240 these conditions, IgA purified from these mice was also sufficient to protect IgA$^{-/-}$ mice from
241 increased tumour load (**Fig. 2j**). Additionally, analyses of recipient faeces during this treatment
242 revealed no coating of the microbiota (**Extended Data Fig. 3a**), raising the possibility that the
243 effect on tumourigenesis is independent of bacterial binding. Consistent with this, recombinant
244 monoclonal secretory IgA specific for influenza HA (CR9114) protected IgA$^{-/-}$ mice from increased
245 tumour formation (**Fig. 2k**). The functionality of this recombinant antibody allowed the
246 investigation of the structural requirements for tumourigenesis suppression. While either
247 secretory or dimeric IgA treatments were sufficient to provide protection, neither the secretory
248 component nor truncated secretory IgA without Fabs, IgG, or monomeric IgA was sufficient (**Fig.
249 2l**). Oral treatments that reduced tumour load mainly reduced the number rather than the size of
250 tumours (**Extended Data Fig. 3b-e**). The dependence of this impact on structure, but not antigen
251 specificity, suggests that IgA might more directly interact with cells that become tumours: the
252 colon epithelium.
253

254 **Impact of IgA on epithelial cells**

255 To further investigate how IgA may affect the steady-state epithelium to influence the probability
256 of tumourigenesis, mid-colon epithelial cells were sorted (live CD45- EPCAM+, **Extended Data**
257 **Fig. 4a**) for single-cell transcriptomics from three IgA$^{+/-}$ mice and three IgA$^{-/-}$ littermates (**Fig.**
258 **3a-b**). Clusters were identified based on known markers, such as stem (*Lgr5*+) and transit-
259 amplifying (*Mki67*) cells partially overlapping in clusters 0, 5, and 9, and goblet cells in clusters 6,
260 8, and 10 expressing the secretory progenitor marker *Atoh1* (**Fig 3a-b**, **Extended Data Fig. 4b**). In
261 terms of cellular composition, IgA$^{-/-}$ mice had more cells in clusters 1 and 5 (**Fig. 3c-d**). Cluster 5
262 represents cycling or early post-mitotic progenitors, as they express the cycling markers *Mki67*
263 and *Nox1* and the canonical Notch target *Hes1* (**Fig. 3b**), which further identifies them as
264 progenitors of the absorptive lineage[53]. The lack of *Muc2* expression is further evidence of their
265 undifferentiated state (**Extended Data Fig. 4b**). Cluster 1 represents a more mature population of
266 colonocytes, however they lack expression of *Aqp8*, the canonical marker for the absorptive cells.
267 Instead, these clusters, as well as their intermediate cluster 4, were marked by the expression of
268 antimicrobials such as *Dmbt1*, *Reg3b*, and *Reg3g* (**Fig. 3b, d**), indicating that they play a more
269 immune-related role. In terms of gene expression, while only a handful of differentially expressed
270 genes distinguished cells from mice by the IgA genotype (**Supplementary Table 3**), these three
271 antimicrobials were the most differentially expressed, with colonocytes from IgA$^{-/-}$ mice
272 expressing higher levels (**Fig. 3e-f, Extended Data Fig. 4c**). These specific genes were previously
273 found to be induced at the single-cell level by bacterial colonization of germ-free mice[54]. At the
274 pathway level, epithelial cells from IgA$^{-/-}$ mice showed a decrease in interferon signalling and an
275 increase in antimicrobial responses, but not a general inflammatory response (**Fig. 3g, Extended**
276 **Data Fig. 4d**). Pathways related to proliferation and central metabolism were upregulated in
277 IgA$^{-/-}$ mice, while adhesion and tight junction pathways had cell type-specific changes (**Fig. 3g**).
278 The highly proliferative cluster 9 exhibited enrichment of the pre-notch reactome in IgA$^{-/-}$ mice
279 (**Fig. 3g**), indicating these cells are beginning to express Notch proteins, steering the cycling cells
280 toward an absorptive fate in the expanded cluster 5. Collectively, analysis of the colon epithelial
281 transcriptome at the single-cell level in IgA$^{-/-}$ mice revealed specific changes in epithelial
282 development related to the expansion of the absorptive progenitor population and enhanced
283 antimicrobial functions.
284

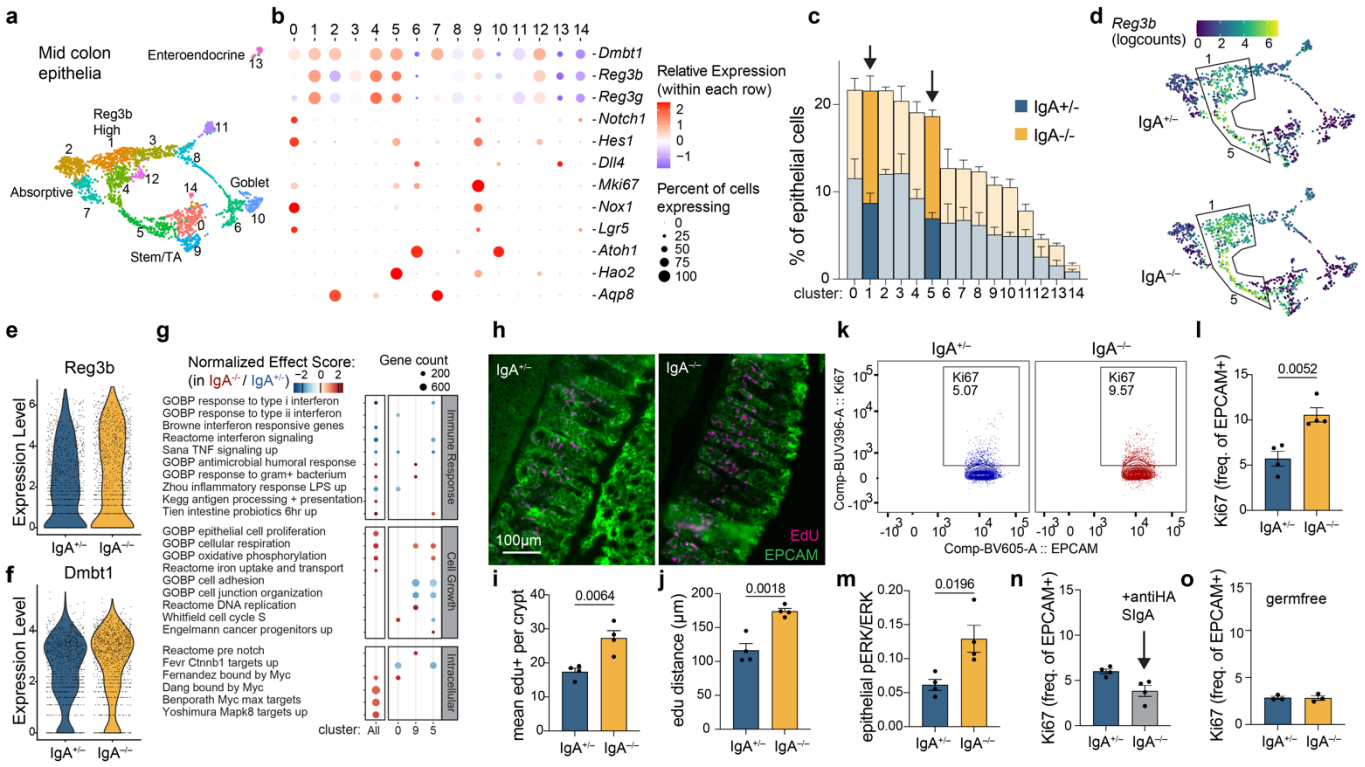

Fig. 3 | Cellular changes in the colon epithelium of IgA$^{-/-}$ mice. a, UMAP and clustering of sorted single colon epithelial cell (live, CD45-, EPCAM+) transcriptomes from IgA$^{+/-}$ and IgA$^{-/-}$ littermates (n = 3 mice per group). **b**, Enrichment of genes of interest across clusters. **c**, Frequency of each cluster of epithelial cells, revealing an increase in cluster 1 and 5 in IgA$^{-/-}$ mice. **d**, Expression pattern of *Reg3b*, the most differentially expressed gene between IgA$^{+/-}$ and IgA$^{-/-}$ littermates is also associated with cluster 1 and 5. **e-f**, Expression of antimicrobials *Reg3b* and *Dmbt1* in all cells by genotype. **g**, Gene set enrichment analyses across all cells and within individual clusters based on IgA genotype revealed a switch from interferon signalling to anti-bacterial pathways, increases in cell cycling, and alterations in intracellular signalling processes. Dots are visible where adjusted p value < 0.05, size of dot represents the number of genes in the pathway, and color represents the normalized enrichment score of that pathway (IgA$^{-/-}$-enriched is positive, red). **h**, Fluorescence microscopy of frozen sections of swiss-rolled mid-colon from mice injected with EdU at 24 and 4 hours prior. **i**, Quantification of EdU positive cells per crypt, and **j**, maximum distance of EdU positive cells from the crypt base, averaged across at least 20 crypts and 5 frames of view per animal (n = 4). **k**, Flow cytometry of colon epithelial cells (CD45-, EPCAM+) with intracellular staining of the cell cycle marker Ki67. **l**, Quantification of the frequency of Ki67+ epithelial cells depending on IgA genotype (n = 4). **m**, ELISA of lysate of isolated colon epithelial cells specific for phosphorylated ERK normalized to the level of total ERK (n = 4). **n**, Ki67 assessment by flow cytometry as before, but IgA$^{-/-}$ mice were gavaged daily with 2.5 µg SIgA for one week (n = 3, 4), or **o**, were rederived germfree (n = 3) (t-tests, p values hidden when p > 0.1).

308 We directly tested whether the developmental and cellularity changes observed by single-cell
309 transcriptomics are due to an overall alteration in the rate of epithelial proliferation in the
310 absence of IgA. Mice were injected with 5-ethynyl-2-deoxyuridine (EdU), which is incorporated
311 into the DNA of dividing cells, 24 h and 4 h before tissue harvest to label all cells proliferating
312 within the timeframe. Using a counterstain of EPCAM (green) to visualize crypt structures, EdU+
313 cells (pink) were quantified in the frozen sections (**Fig. 3h**). Sections from $IgA^{-/-}$ mice had
314 increased numbers of EdU+ cells per crypt (**Fig. 3i**), as well as a greater distance travelled by
315 EdU+ cells away from their origin at the crypt base (**Fig. 3j**), both consistent with an increased
316 overall rate of epithelial proliferation. Isolated epithelial cells from $IgA^{-/-}$ mice also had a higher
317 frequency of intracellular Ki67 measured by flow cytometry (**Fig. 3k-l**), and a higher ratio of
318 phosphorylated ERK normalized to total ERK measured by ELISA (**Fig. 3m**), both independently
319 confirming accelerated epithelial proliferation. Gavage treatment of $IgA^{-/-}$ mice with monoclonal
320 anti-influenza SIgA was sufficient to reduce Ki67 staining to the level observed in $IgA^{+/-}$
321 littermates (**Fig. 3n**). As colon epithelial cycling was previously shown to be a physiological
322 response to microbial stimulation through TLR signalling[55], $IgA^{-/-}$ mice were rederived germ-free
323 to test whether enhanced epithelial proliferation was dependent on the microbiota. In these
324 animals, no IgA-dependent difference was observed in Ki67+ cells measured by flow cytometry
325 (**Fig. 3o**) or in EdU+ cells imaged in frozen sections (**Extended Data Fig. 5a**). This set of
326 experiments establishes that IgA controls colon epithelial cell cycling in mice through a pathway
327 that is dependent on microbiota but not antigen-specificity.
328
329 Plausibly, IgA might impact epithelial proliferation through a direct interaction, which would
330 make antigen specificity irrelevant. To test this possibility, an *in vitro* entero-organoid culture
331 system starting with primary isolated colon crypts was used to mimic normal epithelial
332 developmental processes. Despite the lack of microbial stimulation in culture, high Wnt media and
333 Matrigel optimized to support entero-organoid cultures provide many growth-enhancing
334 signals[56,57]. Colonic crypts isolated from $IgA^{-/-}$ mice were cultured as 3-dimensional organoids,
335 and subsequent treatment with SIgA, but not IgG, reduced the number of organoids recovered
336 (**Fig. 4a-b**). Although independent of bacteria in this sterile culture, this effect of IgA is reciprocal
337 to the physiological stimulation provided by the microbiota that accelerates epithelial
338 proliferation *in vivo*[55]. An anti-proliferative effect of IgA was also observed in a mouse colon
339 epithelial cell line, CMT-93, enabling easier testing of various treatments. Treatment with SIgA, but
340 not IgG, monomeric IgA, secretory component, or no-fab SIgA, was sufficient to slow cell growth
341 (**Fig. 4c**).

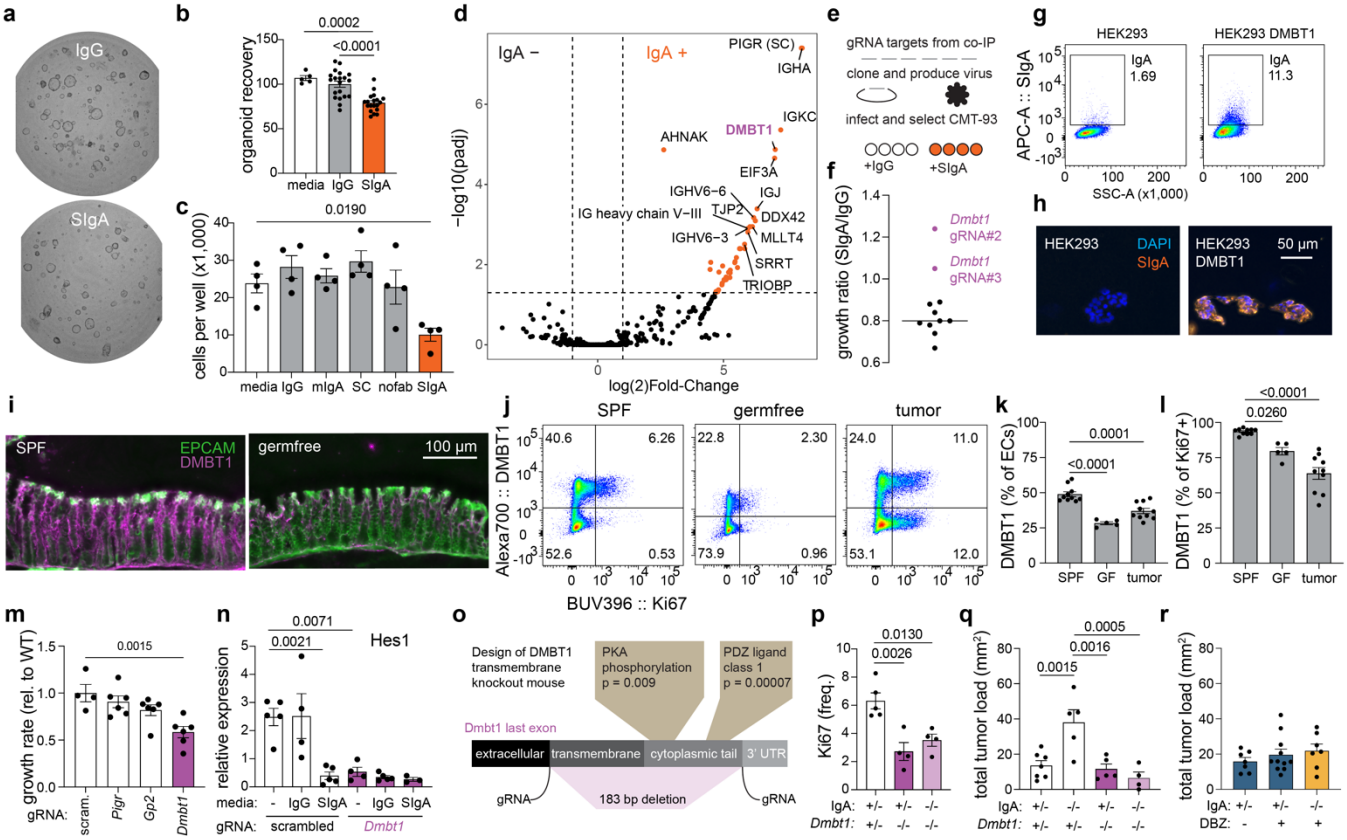

Fig. 4 | SIgA suppresses epithelial proliferation and tumourigenesis via DMBT1. a, Primary mouse colon organoids were cultured from isolated crypts in the presence of indicated antibody isotypes imaged by brightfield microscopy. **b**, Organoid counting from four independent experiments pooled and normalized to the IgG treatment control (n = 5, 20, 19). **c**, CMT-93 mouse colon epithelial cell line cultured with recombinant antibodies for 5 days (n = 4, representative of two independent experiments). **d**, Purified secretory IgA pulldown and mass spectrometry with epithelial organoid lysate (n = 3). **e-f**, Targeted CRISPR screen to discover epithelial surface proteins that are required for regulation of proliferation identifies DMBT1. **g**, Exogenous expression of *Dmbt1* in HEK293 cells confers the ability to bind secretory IgA on the cell surface as assessed by flow cytometry in cells grown in suspension or **h**, imaging of adherent cells (representative of 3 experiments). **i**, Immunofluorescence of DMBT1 in frozen sections of colon (representative of 3 mice). **j**, Flow cytometry measurement of surface DMBT1 and intracellular Ki67 in epithelial cells (live, CD45-EPCAM+) from SPF mice, germfree mice, and tumours isolated from mice 4 weeks after *APC* loss, summarized as the DMBT1+ frequency out of **k**, all epithelial cells, or **l**, proliferating epithelial cells (n = 10, 5, 10). **m**, Growth rate (as a fraction of wildtype) of CMT-93 cells with CRISPR knockouts of indicated genes (n = 4, 6, 6, 6). **n**, qPCR of canonical Notch target, *Hes1*, in CMT-93 cells treated with indicated antibodies for 24 hours (n = 5, 4, 5, 4, 5, 3). **o**, *Dmbt1* last exon genetic structure, intracellular signalling potential, and strategy for a novel mouse knockout of the transmembrane and signalling domains. **p**, Colon epithelial cell proliferation as assessed by flow cytometry of intracellular Ki67 staining in isolated colon epithelial cells from *Dmbt1* signalling knockout mice (pooled two cohorts, n = 5, 4, 4). **q**, Assessment of tumour outcomes four weeks after epithelial-specific loss of *APC* induced in IgA and *Dmbt1* single and double knockouts (pooled two cohorts, n = 7, 5, 5, 4). **r**, total tumour load of mice treated with the Notch inhibitor, dibenzazepine (pooled two cohorts, n = 7, 11, 7)(one-way ANOVA, p values hidden when p > 0.1).

369 Several putative immunoglobulin receptors have been reported to be expressed on colon
370 epithelial cells, but none are known to either bind the secretory form of IgA or regulate
371 proliferation. For an unbiased look at the scope of secretory IgA interacting partners expressed in
372 epithelia, mouse colon organoid lysates were probed with SIgA, which was then purified using
373 magnetic beads. The co-precipitated proteins were analysed by mass spectrometry (**Fig. 4d**).
374 Compared to the control without SIgA, 54 proteins were significantly enriched (**Supplementary**
375 **Table 4**), including the primary components of SIgA: the alpha heavy chain, kappa light chain,
376 secretory component, and jchain. In total, 26 enriched proteins were immunoglobulin-derived. Of
377 the remaining proteins, most were intracellular, but two surface proteins were highly enriched:
378 the antimicrobial DMBT1 and glycoprotein receptor GP2. Interestingly, *Dmbt1* was also one of the
379 three most highly upregulated genes in colon epithelial cells of IgA$^{-/-}$ mice (*see* **Fig. 3f**), and its
380 expression was associated with the absorptive progenitor and anti-microbial colonocyte
381 populations that were expanded in IgA$^{-/-}$ mice (*see* **Fig. 3b, c**). To test whether these candidate
382 immunoglobulin-binding surface proteins are responsible for SIgA-dependent growth
383 suppression, guide RNAs were designed for each in a targeted CRISPR screen that included *Pigr*,
384 *Dmbt1*, and *Gp2* (**Fig. 4e**). As expected, most of the generated CMT93 cells exhibited slower
385 growth when incubated with SIgA compared to IgG (**Fig. 4f**), but two guide RNAs eliminated this
386 phenotype, both of which targeted *Dmbt1*.
387
388 **DMBT1, a regulator of epithelial proliferation that binds IgA**
389 *Dmbt1* (deleted in malignant brain tumours) encodes several large (~200 kDa), highly
390 glycosylated mucin-like proteins in various animal tissues. The human protein was originally
391 described as a bacterial agglutinin and was co-purified as a complex with IgA in saliva[58]. The gene
392 was independently discovered years later and was found to encode a single transmembrane
393 domain on the final exon in both mice and humans[59]. To test whether the expression of membrane
394 DMBT1 is sufficient to confer cell surface IgA binding, HEK293 cells were engineered to
395 overexpress the protein, including the transmembrane domain. Surface expression of the protein
396 was detected by flow cytometry (**Extended Data Fig. 5b**), and this was sufficient to confer cell
397 surface binding of SIgA (**Fig. 4g-h**). In mice, DMBT1 protein was evident in the colon epithelium by
398 immunofluorescence staining (**Fig. 4i**), although the staining was seemingly ubiquitous in the
399 tissue, likely due to secretion. Flow cytometry confirmed the presence of DMBT1 on the surface of
400 the colon epithelial cells (**Fig. 4j**). Expression was induced by microbiota, as colonocytes from
401 germ-free mice exhibited reduced protein levels, as measured by both methods (**Fig. 4i-k**). This is
402 consistent with the notion that IgA controls proliferation via a microbiota-dependent pathway,

403 potentially explaining why, in germ-free conditions, IgA$^{-/-}$ mice display no difference in colon
404 epithelial proliferation (*see* **Fig. 3o**). Cell surface DMBT1 expression was also strongly associated
405 with proliferation, as almost all Ki67+ epithelial cells were DMBT1+ (**Fig. 4l**). This association was
406 lost in tumour cells isolated from the *APC*-driven model (**Fig. 4l**), which is consistent with the
407 inability of IgA to regulate tumour growth. Next, we explored the functional relationship between
408 DMBT1 and epithelial proliferation using *in vitro* and novel mouse models.
409
410 *Dmbt1* $^{-/-}$ epithelial cell lines had slowed growth, indicating that DMBT1 is an activator of
411 proliferation (**Fig. 4m**). As our analysis of IgA impacts on colon epithelial cells implicated the
412 Notch-dependent growth of absorptive progenitors[60] (**Fig. 3b-c**), we assessed the expression of
413 the canonical Notch target, *Hes1*, in the reductionist *in vitro* model. *Hes1* expression was
414 substantially decreased upon DMBT1 knockout, linking DMBT1 to Notch ligand binding or signal
415 transduction (**Fig. 4n**). Additionally, treatment of wild-type cells with SIgA, but not IgG, had the
416 same effect on Notch signalling (**Fig. 4n**). However, treatment of *Dmbt1*$^{-/-}$ cells with SIgA had no
417 further effect, placing DMBT1 downstream of SIgA in a pathway regulating Notch-dependent
418 proliferation. Thus, DMBT1 has potential intracellular signalling activity that is likely distinct from
419 its antimicrobial functions.
420
421 To specifically interfere with its role as a signalling receptor, we designed a mouse carrying a
422 mutation in the last exon of *Dmbt1* that removed its transmembrane domain and cytoplasmic tail
423 (**Fig. 4o**). To test the role of DMBT1 in specific IgA-related phenotypes *in vivo*, we crossed this
424 transmembrane knockout to IgA$^{-/-}$ and IgA$^{-/-}$ *Cdx2*^{CreER}*APC*$^{fl/fl}$ mice. Compared to littermate
425 heterozygous controls, *Dmbt1* $^{-/-}$ mice showed decreased proliferation (**Fig. 4p**), consistent with
426 its role as an activator of proliferation. IgA$^{-/-}$ mice in this background showed no increase in
427 proliferation, indicating that DMBT1 activation of proliferation is required for IgA modulation
428 (**Fig. 4p**). Finally, we tested the role of DMBT1 in IgA$^{-/-}$ susceptibility to *APC*-driven tumours.
429 While IgA$^{-/-}$ mice still exhibited increased tumours in a *Dmbt1*$^{+/-}$ context, knockout of *Dmbt1*
430 signalling in littermates completely reverted IgA$^{-/-}$ susceptibility (**Fig. 4q**). The epistatic nature of
431 interfering with DMBT1 signalling *in vivo* is consistent with this being the mechanism whereby IgA
432 suppresses epithelial proliferation and tumourigenesis.
433
434 We are left with a pathway in which IgA binds to and suppresses functions of DMBT1, which itself
435 stimulates Notch-dependent epithelial proliferation, increasing the probability of tumour
436 initiation. This would predict that the susceptibility of IgA$^{-/-}$ mice to colorectal tumours is

437 effectively Notch-dependent. Gamma secretase inhibitors such as dibenzazepine (DBZ) prevent
438 Notch receptor cleavage and have been shown to reduce proliferation of intestinal epithelial
439 cells[61]. We designed an experiment to inhibit Notch in IgA$^{+/-}$ or IgA$^{-/-}$ *Cdx2*^{CreER}*APC*$^{fl/fl}$ mice within
440 the early therapeutic window used for oral treatment with IgA (**Extended Data Fig. 5c**). While
441 this low-dose treatment just 5 days before and 5 days after APC loss did not affect the tumour
442 outcome in IgA$^{+/-}$ mice, IgA$^{-/-}$ littermates were now indistinguishable (**Fig. 4r**). This confirms that
443 Notch-dependent outgrowth of absorptive progenitors during steady state, initially observed by
444 single-cell RNA-Seq (**Fig. 3**), is responsible for increased tumourigenesis in IgA$^{-/-}$ mice.
445

446 **Discussion**

447 We found that by modulating DMBT1-induced proliferation of colon epithelial cells, IgA in the
448 lumen of the gut lowers the risk of colon tumour initiation in mouse models. IgA was previously
449 reported to suppress the growth of ovarian tumours through interactions with immune cells and
450 pIgR, which is highly expressed in ovarian tumours[62]. In contrast, pIgR is dramatically
451 downregulated in human colorectal tumours[63], and we observed an effect of IgA only on
452 physiological cell growth with no dependence on *Pigr*, supporting the concept of distinct functions
453 of IgA in each tissue context. Faecal IgA levels have been reported to be elevated in colorectal
454 cancer patients[64], although the functional roles of IgA in colorectal cancer have been mostly
455 unexplored. Consistent with our model, a recent study independently reported the susceptibility
456 of IgA$^{-/-}$ mice to AOM-DSS-induced tumours[65]. Unlike other body sites, there is substantial
457 evidence for a bacterial role in tumour initiation in the colon[66], which may be related to
458 physiological interactions between the microbiota and epithelium and mediator molecules such as
459 IgA and DMBT1. Interventions that can prevent tumour emergence in gastrointestinal cancers are
460 lacking beyond general guidance regarding healthy diet and lifestyle, although post-polypectomy
461 patients present a potential therapeutic window that has yet to be exploited. In an extensive
462 proteomics analysis of colon polyp biopsies, DMBT1 loss at the protein level distinguished
463 dysplasia from normal epithelium and predicted future progression to cancer[67], confirming earlier
464 reports that DMBT1 protein loss in tissue was associated with poor prognosis in both colorectal[68]
465 and prostate[69] cancers. This is also consistent with our findings in animal models that DMBT1 is
466 associated with physiological proliferation and absorptive lineage development, whereas
467 transformed adenomas with dysregulated Wnt will escape DMBT1-IgA regulation of Notch-
468 dependent growth.
469

470 Despite these effects on tumourigenesis, the main function of IgA-DMBT1 in the regulation of cell
471 cycling seems to be homeostatic. Just as IgA is produced in response to microbial colonization,
472 DMBT1 is known as an antimicrobial that is regulated by bacterial signals transduced via NOD2
473 and Toll-like Receptors[70]. Induction of epithelial expression of DMBT1 by bacteria has been
474 demonstrated not only in mammals[54] but also in corals[71], suggesting an evolutionarily ancient
475 (preceding immunoglobulin) relationship between this receptor and epithelial responses to
476 microbiota. DMBT1 was previously shown to promote proliferation of endothelial cells (also
477 Notch-dependent)[72] and was correlated with epithelial proliferation in the context of *Citrobacter*
478 *rodentium* pathogenesis[73]. As part of an inflammatory response, DMBT1 is upregulated in both
479 Crohn's Disease and Ulcerative Colitis, and total DMBT1 knockout mice were found to be more
480 susceptible to mouse models of colitis[74]. This and other induced antimicrobial functions of
481 epithelial cells must be regulated at steady state to avoid overreaction to the commensal
482 microbiota. The present study establishes a homeostatic feedback mechanism whereby IgA
483 inhibits the ability of DMBT1 to activate epithelial proliferation. In the absence of IgA, DMBT1
484 induces the proliferation of absorptive progenitors with antimicrobial functions. This mechanism
485 may also explain early microarray experiments of small intestinal samples from B cell-deficient,
486 IgA$^{-/-,}$ and *Pigr*$^{-/-}$ mice, which detected increased expression of genes encoding antimicrobial
487 peptides[24,75]. While the role of IgA in shaping microbiota form and function is well established, this
488 direct interaction with epithelial cells via DMBT1 seems to be a parallel function. As microbial
489 stimulation of epithelial cells provides an "accelerate" signal for proliferation and antimicrobial
490 function, IgA feedback appears to be a "brake" to modulate these behaviours, closing the
491 homeostatic loop of host responses to microbiota.
492
493 The incredible quantity of IgA secreted into the lumen at steady state is sufficient to support
494 multiple functions. Despite coating a substantial fraction of the microbiota at the cellular level, IgA
495 remains in excess at the luminal surface. It is estimated that approximately 95% of IgA in the
496 intestinal lumen is unbound[76] and is, therefore, presumably available for epithelial feedback.
497 Alterations in epithelial responses to microbiota may be a primary consequence of total mucosal
498 IgA deficiency, a human condition that remains mysterious and difficult to study. The impacts of
499 IgA on microbiota, as well as on epithelia described here, may intersect with other genetic and
500 environmental factors to manifest in patient-specific outcomes[4,7,10,11,77].
501

502 **Author contributions**

503 G.P.D. and D.M. conceived and initiated the project. G.P.D. designed and performed most of the
504 experiments, with guidance from D.M.. G.L.R. performed organoid experiments, purified IgA,
505 performed the pull-down assay, and assisted with most of the experiments. M.S. performed the
506 colonoscopy procedures and cultured organoids. C.W. assisted with tissue culture and binding
507 experiments. G.P.D. analyzed 16S rRNA amplicon sequencing, I.M. analyzed single-cell RNA-Seq,
508 and G.C. analyzed bulk RNA-Seq, with guidance and analysis oversight from T.B.R.C. N.L.D. assisted
509 with flow cytometry and tissue culture experiments and C.H. assisted with fluorescence imaging.
510 D.Z. and B.M.S. designed and produced recombinant secretory component and IgA variants. G.P.D.,
511 B.A., and B.S.R designed and executed the epithelial cell sorting and single-cell RNA-Seq. S.G.,
512 B.S.R., S.F.T., B.M.S., G.D.V., and D.M. supervised and guided the experimental design and
513 interpretation. G.P.D. and D.M. wrote the manuscript, and all authors edited the manuscript.
514

515 **Acknowledgements**

516 The authors thank S. Tavazoie (Rockefeller), J. Faith (Mt. Sinai), D. Wesemann (Brigham and
517 Women's), M. Koch (Fred Hutchinson), L. Mesin (Rockefeller), and members of the Mucida and
518 Victora labs at Rockefeller University for useful discussions. S. Leonard assisted with protein
519 purifications at University of Illinois. Germ-free mice were generated and maintained by A. Rogoz
520 at Rockefeller University. DMBT1 transmembrane-knockout mice were generated by J. Bortolatto
521 at Rockefeller University. All animals were monitored and cared for by the staff of the
522 Comparative Bioscience Center at Rockefeller University. Sequencing was performed at the
523 Genomics Resource Center of Rockefeller University (RRID:SCR_020986). Proteomics data were
524 generated by the Proteomics Resource Center at Rockefeller University (RRID:SCR_017797) with
525 assistance from H. Molina using instrumentation funded by the Sohn Conferences Foundation and
526 the Leona M. and Harry B. Helmsley Charitable Trust. G.P.D. was a Robert Black Fellow of the
527 Damon Runyon Cancer Research Foundation (DRG-2362-19). G.L.R. was supported by a
528 scholarship from Fundação Maria Emília (Brazil). Project initiation was supported by pilot grants
529 from the Rockefeller University Center for Basic and Translational Research on Disorders of the
530 Digestive System through the generosity of the Leona M. and Harry B. Helmsley Charitable Trust
531 and the Shapiro-Silverberg Fund for the Advancement of Translational Research to G.P.D. The
532 project was funded by grants from the NIH to the B.M.S.. (R01AI165570) from the NIH to G.D.V.
533 and D.M. (R01AI157137), and D.M. (U54CA261701). G.D.V. and D.M. are investigators of the
534 Howard Hughes Medical Institute.
535

536 **Competing interests**

537 The authors declare no competing interests.

538

539 **Methods**

540 Mice

541 All mice were housed at the Rockefeller University and handled in accordance with protocols
542 approved by the Institutional Animal Care and Use Committee (IACUC) and under the ethical
543 guidelines within the National Institutes of Health Guide for the Care and Use of Laboratory
544 Animals. C57BL/6J (000664) and *Cdx2*^{CreER} (022390) mice were purchased from Jackson
545 Laboratories. *IgA*$^{-/-}$ mice on a C57BL/6J background were provided by Margaret Conner (Baylor)
546 and *APC*$^{fl/fl}$ mice on a C57BL/6J background were provided by Sergei Grivennikov (Cedars-Sinai).
547 These mice were housed in Specific Pathogen Free conditions on a fixed 12 hour light-dark cycle
548 with food and water provided *ad libitum*. *IgA*$^{-/-}$ mice were rederived by c-section into germfree
549 flexible film isolators (Class Biologically Clean) that were routinely monitored by quantitative real
550 time PCR. Germfree mice were housed with a fixed 12 hour light-dark cycle with autoclaved food
551 and water provided *ad libitum*. The genotype of mice was determined by quantitative real time
552 PCR analyses by Transnetyx. The IgA genotype of mice was routinely cross-checked using ELISA
553 or flow cytometry. For experiments comparing IgA$^{+/-}$ to IgA$^{-/-}$, littermate, sex-matched controls
554 were co-housed from weaning through the duration. During data collection, mice were identified
555 only by an experiment name, cage number, and ear punch, which was matched to genotype post
556 hoc. Experiments were initiated when mice were aged 8-10 weeks, unless otherwise noted. Both
557 male and female mice were used for all experiments, analyzed separately, and then pooled if no
558 sex differences emerged. Estrous cycle was not controlled for.

559

560 Murine cancer models

561 For all cancer models, animals were monitored daily for sickness behavior and weighed at least
562 twice per week to assess health and maintain a humane endpoint if weight loss exceeded 20% of
563 their initial weight. For the APC model, *Cdx2*^{CreER}*APC*$^{fl/fl}$ mice were injected intraperitoneally at day
564 0 and day 3 with 0.8 mg tamoxifen (Sigma) from a stock solution at 4 mg/ml dissolved in corn oil
565 (Sigma). After 4 weeks (day 28), mice were sacrificed to count and measure tumours. For the
566 AOM-DSS model, mice were injected intraperitoneally with 12.5 mg/kg azoxymethane (AOM) at
567 day 0. Exposure to 1.5% dextran sodium sulfate (DSS) in drinking water replaced their normal
568 water for 1 week starting at day 0. This was followed by a 2 week break, a second DSS exposure
569 for 1 week, a 2 week break, and a third exposure for 1 week. Animals were sacrificed at day 100 to

570 measure and count tumours. Lipocalin-2 was measured using the Mouse Lipocalin-2/NGAL
571 DuoSet ELISA kit from R&D Systems (Cat. DY1857) according to manufacturer's protocol. For the
572 pre-cancerous organoid implant model, $IgA^{+/-}$ and $IgA^{-/-}$ mice were injected with 1.5 $x10^5$ cells of
573 AKPS organoids (*APC*, *Kras*(G12D), *P53*, *Smad4*; generated in Sergei Grivennikov's laboratory).
574 Cells were injected over 3 injections (5 $x10^4$ cells in 40 uL each), spaced ~ 0.5 cm apart in the
575 distal colon and rectum wall using a colonoscope (Karl Storz, Model TC300) with a custom-made
576 33-gauge needle (Hamilton Company). AKPS organoids were cultured by resuspending organoid
577 cells in 50% matrigel (Corning) in cold ADF^+ media (Advanced DMEM F12 (Invitrogen)
578 supplemented with 5% heat inactivated FBS (Sigma-Aldrich), 1% Penicillin-Streptomycin-
579 Glutamine (Invitrogen), 1% HEPES (Invitrogen)). In a 6-well plate, 40 uL droplets of cell
580 suspension were plated and incubated at 37°C for 20 minutes, followed by adding 3 mL of pre-
581 warmed ADF^+ media. To prepare cells for injections, AKPS organoids were dissociated with cold
582 ADF^+ media to break down matrigel, and spun down at 350g for 5 minutes. Organoid pellet was
583 resuspended in Tryple Express Enzyme (Thermo Fisher Scientific) and incubated at 37°C for 30
584 minutes with shaking at 120 rpm. Organoids were further broken down into cells by pipetting
585 multiple times with P1000, followed by washing with ADF^+ media and spinning down at 350g for
586 5 minutes. Cells were resuspended in ADF^+ media for counting, then volume was further adjusted
587 to keep cells at 1250 cells/uL in 10% matrigel, 1% filter-sterilized Methylene Blue (Biopharm,
588 Amazon), and 10 uM Y27632 (Stemcell Technologies). Implanted tumours were monitored every
589 two weeks using the colonoscope and were scored according to a previously published system (1:
590 small but detectable tumour, 2: tumour covering one-eighth of colon circumference, 3: tumour
591 covering one-fourth of colon circumference, 4: tumour covering one-half of colon
592 circumference)[78].
593
594 Interventions in APC cancer model
595 For antibiotic depletion of the microbiome, mice were provided with sterile-filtered drinking
596 water with 1 mg/ml ampicillin, 1 mg/ml neomycin, 0.5 mg/ml vancomycin, and 0.5 mg/ml
597 metronidazole, supplemented with 10 mg/ml sucralose for palatability. For oral gavage
598 treatments to rescue IgA deficiency, mice were subjected to a daily intra-gastric gavage with 2.5 μg
599 of IgA (or the equivalent) in 200 μl PBS. For Notch inhibition, mice were given a daily 3 μmol/kg
600 intraperitoneal injection of dibenzazepine (DBZ) (StemCell Technologies) which was first
601 dissolved as a 10 μmol/ml in DMSO stock solution (kept frozen at -20C) and then diluted in 0.5%
602 hydroxypropyl methylcellulose for injection.
603

604 Bulk RNA-Seq
605 Working on ice with one animal at a time until samples were homogenized by bead beating to
606 stabilize RNA, mice were sacrificed by cervical dislocation, the colon was dissected, cut open
607 longitudinally, and washed 3 times in PBS to remove lumen contents. An approximately 0.5 cm x
608 0.5 cm sample of tissue from the mid-colon (3 cm distal from the cecal junction) was collected in a
609 Lysing Matrix D tube (MP Biomedicals) with 1 ml Trizol (Invitrogen) and beat at max speed for 60
610 seconds (MP Biomedicals FastPrep 24 Bead Beater), twice, with 5 minutes rest on ice between.
611 Total RNA was purified according to the manufacturer's instructions for Trizol, followed by
612 further purification using a Qiagen RNeasy column with on-column DNase treatment (Qiagen)
613 according to the manufacturer's instructions. RNA quality was assessed using an Agilent
614 Bioanalyzer and only samples with RIN > 8.0 were used for poly-A selected mRNA-Seq. Libraries
615 were sequenced on an Illumina NextSeq 500 high-throughput flow cell, with a single-end 75 bp
616 read, yielding between 23 and 30 million high quality paired-end reads per sample. STAR aligner
617 2.7.10a and biomaRt 2.52.0 were used to align reads and annotate genes with the GRCm39 mouse
618 genome and M32 mouse transcriptome. Differential expression analyses was performed using
619 DESEq2 1.36.0 and gene set enrichment analyses using fgsea 1.22.0 with gene sets
620 c2.cgp.v7.5.1.symbols and c5.go.bp.v7.5.1.symbols.
621
622 16S rRNA amplicon sequencing
623 Mice were sacrificed by cervical dislocation and the colon was dissected and opened longitudinally
624 on ice using autoclaved tools and aseptic technique. Lumen samples were taken from the mid
625 colon, then the tissue was washed thoroughly 3 times in sterile PBS on ice, dabbed several times
626 on a sterile petri dish to dry, and mucus was gently scraped from the tissue using a plastic cell
627 scraper. All samples were frozen and -80C prior to further processing. DNA extraction was
628 performed using the QIAamp PowerFecal Pro DNA Kit (Qiagen) with bead beating on an MP
629 Biomedicals Fastprep 24, according to manufacturer's protocols. To avoid contaminating the
630 lower biomass samples, mucus samples were processed separately, with decontamination of
631 benches, racks, pipettes, and microcentrifuge prior to processing. 16S rRNA was amplified and
632 libraries were prepared and pooled according to the Earth Microbiome Project 16S Illumina
633 Amplicon protocol (earthmicrobiomeproject.org). Sequencing was performed with an Illumina
634 MiSeq 150 bp paired-end run. The data were analyzed using the Qiime 2 (v2022.8) package.
635 Amplicon sequence variants (ASVs) were identified and chimeric sequences were removed using
636 Deblur. Phylogenetic analyses were performed using the Qiime 2 classifier trained on the SILVA
637 database (v138) from 515F to 806R to match the amplicon sequencing. Following the Deblur

638 processing, only samples with more than 1000 reads were included and only features with at least
639 100 reads across all samples that were present in at least 5 different samples were included.
640
641 Faecal IgA purification
642 Similar to a previously published method[79], the small intestine, cecum, and colon were dissected
643 from three healthy animals, and the contents were pooled into a 15 mL conical tube. To the pooled
644 contents, 6 mL of 1× PBS-T (PBS with 1% Tween 20, prepared from 10× stock (AlfaAesar))
645 containing a protease inhibitor cocktail (Roche) was added. The mixture was vortexed at
646 maximum speed for 5 minutes. After vortexing, the suspension was centrifuged at 3000 g for 10
647 minutes. The supernatant was then divided into six 2 mL tubes, which were centrifuged again at
648 10,000 g for 10 minutes. During this second centrifugation, Protein L magnetic beads (Pierce™
649 Protein L Magnetic Beads, Thermo Scientific) were prepared. The bottle of beads was gently
650 vortexed to mix, and 200 µL of Protein L beads was added to each of the six 2 mL tubes, followed
651 by the addition of 300 µL of PBS-T. The tubes were vortexed gently for 1 minute, after which the
652 beads were collected using a magnet, and the supernatant was removed. This wash step was
653 repeated by adding 1 mL of PBS-T, vortexing gently for another minute, and collecting the beads
654 with a magnet to remove the supernatant. Following the beads' preparation, the IgA supernatant
655 was transferred into the tubes with the washed Protein L beads. The mixture was shaken gently at
656 room temperature for 1 hour to allow for binding. After incubation, the beads were collected using
657 a magnet rack, and the supernatant was discarded. The beads were then washed three times with
658 1 mL of PBS-T, gently vortexed for 1 minute during each wash, followed by collection of the beads
659 with a magnet and removal of the supernatant. To elute the bound IgA, 200 µL of elution buffer
660 (0.1 M glycine at pH 2-2.5) was added to the beads. The tubes were gently vortexed and incubated
661 at room temperature for 10 minutes, with occasional gentle vortexing. The beads were then
662 collected with a magnet, and the supernatant containing the eluted IgA was combined into a new
663 tube. To neutralize the pH of the eluted IgA, an appropriate volume of neutralization buffer (10%
664 1 M Tris-HCl at pH 8) was added. Concentration was checked using a Nanodrop (for crude
665 measurement) or an ELISA assay. Finally, purified IgA was sterile filtered through a 0.22 µm filter.
666
667 Monoclonal IgA and structural variant generation
668 Recombinant secretory component, CR9114 SIgA, and all structural variants were produced
669 following previously published methods[80]. Briefly, genes encoding the *mus musculus* IgA heavy
670 chain constant region (Uniprot P01878) and the lambda light chain constant region (Uniprot
671 A0A0G2JE99) were fused with the CR9114 VH and VL domain sequences[81] to create complete

672 heavy chain and light chain sequences. Alternatively, the *mus musculus* IgA heavy chain constant
673 region domains CH3 and CH4 were fused to an N-terminal hexahistine tag to create a Fc(no fabs)
674 expression construct. The TPA signal sequence (residues MDAMKRGLCCVLLLCGAVFVSPAGA) was
675 encoded at the start of the heavy chain sequences and the mouse IgKappa signal sequence
676 (residues METDTLLLWVLLLWVPGSTG) was encoded at the start of the light chain sequence.
677 These sequences, along with *mus musculus* JC (Uniprot P01592; native signal peptide) and *mus*
678 *musculus* pIgR ectodomain (SC) residues 1-567 (Uniprot O70570; native signal peptide) with C-
679 terminal hexahistine affinity tag sequence, were cloned into mammalian expression vector
680 pD2610v1 (Atum). Resulting expression constructs were transiently transfected or co-transfected
681 into HEK Expi-293-F cells with the ExpiFectamine 293 transfection kit (ThermoFisher, A14525),
682 according to company protocol. Resulting proteins were purified via CaptureSelect LC-lambda
683 (mouse) affinity matrix (ThermoFisher, 194323010) or Ni-NTA agarose (Qiagen, 30210), and by
684 Superose 6 Increase 10/300 GL (Cytiva Life Sciences, 29091596) size exclusion chromatography
685 using an ÄKTA pure 25 chromatography system (Cytiva Life Sciences). Purified proteins were
686 exchanged into 1x phosphate buffered saline buffer (HyClone, SH30258.01) prior to use in
687 experiments.
688
689 Colon epithelial cell isolation
690 Mice were sacrificed by cervical dislocation. The colon was dissected on ice and opened
691 longitudinally. Lumen content was gently removed and the tissue was washed 3 times in ice cold
692 PBS. The mid colon was taken for further processing (a length of the tissue starting from 3 cm
693 distal from the cecal junction and continuing for 4 cm toward the rectum). The tissue was cut into
694 1 cm pieces into PBS with 30 mM EDTA and 1.5 mM DTT and incubated on ice for 20 minutes with
695 a brief shake at the end to remove mucus. The tissue was moved to DMEM with 30 mM EDTA and
696 2% fetal calf serum and incubated at 37C in a waterbath for 10 minutes with an aggressive shake
697 for 30 seconds at the end to remove epithelial cells from the tissue. The cells in media were
698 collected after passage through a metal sieve to remove remaining tissue. Pelleted cells were
699 washed once with HBSS with 10% FCS then resuspended in HBSS (with divalent cations) with 200
700 µg/ml dispase II (Sigma D4693) and incubated for 10 minutes at 37C in a water bath with brief
701 shaking every 2 minutes to dissociate epithelia into a single cell solution (confirmed by light
702 microscopy). The reaction was stopped by adding FCS to 10% and mixing by inversion. Cells were
703 filtered through a 70 µm filter and washed with HBSS 10% FCS. Cells were stained for flow
704 cytometry in a complete T cell media: RPMI-1640 (Gibco 21870) plus 10% fetal bovine serum
705 (Gibco10437), 1% Pen/Strep (Gibco15140), 1% L-glutamine (Gibco25030), 1% NaPyruvate

706 (Gibco113690), 1% Nonessential amino acids (Gibco 11140), 1% HEPES (Gibco 15630) and 2-
707 Mercaptoethanol [50uM] (Aldrich M6250). For intracellular staining, cells were fixed,
708 permeabilized, and stained using the eBioscience Foxp3 Transcription Factor Staining Buffer set
709 according to the manufacturer's recommendations.
710
711 Single cell RNA-Seq
712 Epithelial cells isolated as described above (Colon epithelial cell isolation) were stained with
713 individual Biolegend TotalSeq C antibodies (1:100) to allow for sample-level barcoding. Epithelial
714 cells (SSC, FSC, live, CD45-, EPCAM+) were sorted on a BD FACSAria III Cell Sorter using a 70 µm
715 nozzle at 45 psi, pooling 20,000 cells per sample together in one tube (total 120,000 cells). Post-
716 sort viability was estimated to be 90% by trypan blue staining. A sample of the cell mixture was
717 loaded into a single well of the 10X Genomics Chromium microfluidic device. A single-cell gene
718 expression library was generated following the manufacturer's protocol for a Chromium Next
719 GEM Single Cell 5' Reagent Kit v2 (Dual Index) with Feature Barcode technology for Cell Surface
720 Protein (to capture the TotalSeq C sample barcodes). Libraries were sequenced on a NovaSeq S1
721 flow cell. Primary analysis, encompassing alignment and generation of feature barcodes matrices,
722 was performed on Cell Ranger (v7.0.1), which showed 2,764 cells captured with a mean of
723 152,000 reads and 2,915 genes per cell. Cell Ranger was run with the option `--feature-ref=` to add
724 the sequence information of the first six barcodes on TotalSeq C, the first three corresponding to
725 $IgA^{+/-}$ samples and the last three to IgA−/− mice, according to the manufacturer recommendations.
726 Filtered feature barcode matrices were then imported to the R environment using Seurat (v4.3.0)
727 and all further analyses were done in R. Cells were filtered by singlet hashtag status, percentual of
728 mitochondrial gene expression less than 10% and maximum RNA count per cell to avoid doublets
729 and dying cells, then were scaled by SCT transform and all the PCA, UMAP and clustering
730 possibilities were calculated. Final clustering resolution was decided according to biological
731 difference between epithelial cell types and cell type annotation was performed using enrichment
732 packages as ClusterProfiler (v4.6.2) and fgsea (v1.24.0) and manual curation. Differential
733 Expression was perfomed using the FindMarkers function in Seurat. Graphs were plotted using
734 Seurat functions, iSEE visualization package (v2.10.0) and ggplot2 (v3.4.3). Final functional
735 enrichment for figures was done using fgsea (v1.24.0) against GO BP and msigdb mice c2
736 databases (c2.cgp.v7.5.1.symbols and c5.go.bp.v7.5.1.symbols).
737
738 Measurements of *in vivo* epithelial proliferation (EdU, Ki67, pERK)

739 Mice received 500 µg of 5-ethynyl 2'-deoxyuridine (EdU) (Thermo Fisher A10044) in a 100 µl PBS
740 intraperitoneal injection at 24 hours and 4 hours prior to sacrifice. The colon was dissected on ice,
741 opened longitudinally, and lumen content was gently removed with forceps. Swiss rolls of colon
742 tissue were fixed in PBS-buffered 2% PFA for 2 hours at 4C, washed three times with PBS, and
743 frozen in OCT. A cryostat was used to cut 16 µm sections which were adhered to Superfrost Plus
744 White slides (Fisherbrand). Edu was visualized using the Click-iT EdU Alexa Fluor 647 Imaging Kit
745 (Thermo Fisher) according to the manufacturer's protocol, including a counterstain with 1:200
746 AF488 anti-mouse CD326 (EPCAM) (Biolegend Cat#118210). Stained sections were mounted with
747 Fluoromount G (Southern Biotech) and imaged on a Keyence BZ-X800 epifluorescence
748 microscope. Crypts were assessed in the mid-colon region (only the middle third of the length of
749 the colon) and only counted when both the bottom and top of the same crypt was clearly
750 discernable by EPCAM staining. At least 5 fields of view and at least 20 crypts were counted for
751 each sample. For Ki67 staining, epithelial cells were prepared from mid colon samples as
752 described above (Colon epithelial cell isolation) and analyzed on a BD FACSymphony.
753 Phosphorylated ERK was measured by preparing epithelial cells as described above (Colon
754 epithelial cell isolation) and using a Phospho-Erk1 (pThr202 / pTyr204 + Erk2 (pTyr185/187)
755 and pan-Erk1 / 2 ELISA Kit from Sigma (Cat. RAB0349) according to manufacturer's instructions.
756
757 Isolation and culture of mouse-derived colon organoids
758 Crypts were isolated from the colons of IgA knockout mice through successive 30-minute and 1-
759 hour incubations at 4°C in PBS containing 10 mM EDTA, according to a published method[82]. After
760 isolation, the cells were cultured in a hybrid medium composed of 50% primary medium
761 (DMEM/F12 supplemented with 1% HEPES (Gibco 15630), 1% L-glutamine (Gibco25030), 1%
762 Pen/Strep (Gibco15140), 20% fetal bovine serum (Gibco10437)) and 50% conditioned L-WRN
763 medium, further enriched with 50 ng/mL EGF (Sigma SPR 3196-500). Crypts in hybrid media
764 were mixed with matrigel (Fisher Scientific CB40230C) (30-50%) and dispensed into a 48-well
765 plate, with each well receiving 200 µL of the mixture. The plate was incubated for 20 minutes at
766 37°C. After this period, 300 µL of enriched hybrid media was added to the top of each well.
767 Following three days, 200 uL of enriched hybrid media was added to each well, and slow growth
768 of cells was observed for two more days. For passaging, organoids were dissociated by incubation
769 in TrypLE™ (Thermo Fisher Scientific 12605010). For subsequent culture, the cells were placed in
770 the enriched hybrid media mixed with matrigel (30-50%). A volume of 40 µL of the cell-matrigel
771 suspension was dispensed into 5 distributed drops per well in a 6-well plate. The plate was
772 incubated to polymerize the matrigel at 37°C for 5 minutes and then inverted for 15 minutes to

773 prevent cell attachment to the bottom of the plate surface. Treatments with antibodies [10ug/mL],
774 including IgA purified from faeces and mouse IgG2a isotype control (BioXCell BE0085), were
775 embedded in supplemented hybrid media and placed in their respective wells. The media was
776 changed after 3 days. Imaging was performed for 4 days after adding treatments using Z-stack on
777 a Keyence BZ-X800 epifluorescence microscope. Image quantifications were made manually using
778 ImageJ 2.14.0.
779
780 Tissue culture:
781 CMT-93 cells (CCL-223, ATCC), adherent HEK293 cells, and Expi293F cells were grown in high-
782 glucose DMEM (4 mM L-glutamine, 4500 g/L glucose, 1 mM sodium pyruvate, and 1500 mg/L
783 sodium bicarbonate) supplemented with 10% FBS. Media was changed every two days. HEK293
784 cells were transfected using X-tremeGENE9 (Roche) with a pCMV6 mammalian expression vector
785 carrying a full-length *Dmbt1* gene (Origene MR212101). Cells were analysed 3 days post-
786 transfection by staining with recombinant anti-HA SIgA labelled with alexa fluor 647 for imaging
787 or with a rat anti-mouse DMBT1/GP340 antibody (clone 548031) for flow cytometry. The CMT-93
788 cells were used between passage number 5 and 20 post-ATCC handling. Treatments with
789 antibodies were initiated immediately upon plating cells and were kept in media for five days,
790 with one media change. At the endpoint, cells were counted using a flow cytometer analyser with
791 counting beads and a live/dead stain (which we found to be more reproducible than manual or
792 automated counting of trypan blue). CRISPR knockouts were performed using the lentiCRISPR
793 system as previously described[83]. Briefly, guide RNAs were cloned into lentiCRISPR v2 plasmid
794 (addgene #52961), adherent HEK293 cells were transfected using X-tremeGENE9 (Roche) reagent
795 with individual lentiCRISPR plasmids and packaging vectors (VSV-G and Delta-VPR) to produce
796 virus particle-containing supernatants. CMT-93 cells at 30-50% confluence were infected with
797 individual viral supernatant by centrifuging for 90 minutes at 2200 rpm at room temperature and
798 then incubating for 24 hours at 37C. Cells were selected with 5 μg/ml puromycin for the following
799 24 hours, after which they were provided with fresh media and treatment was initiated. RNA was
800 isolated from tissue-cultured cells using Trizol and Qiagen RNeasy kits as described above (bulk
801 RNA-Seq), first-strand cDNA synthesis was performed using the BioRad iScript kit, and
802 quantitative real-time PCR was performed using Power SYBR Green PCR Master Mix (Applied
803 Biosystems) on a QuantStudio 3 (Applied Biosystems). All primers and guide RNAs are listed in
804 **Supplementary Table 5**.
805
806 IgA co-purification and mass spectrometry

807 Colon organoids derived from IgA knockout mouse, *ApcΔ/Δ*;*Kras*$^{G12D/+}$;*Trp53Δ/Δ* (AKP)[84] and
808 metastatic organoids (both generated in Omer Yilmaz's laboratory) were cultured for use in
809 cellular lysate preparation. The IgA knockout mouse-derived organoids were isolated as
810 previously described in this methods section, but this time cultured with IntestiCult™ Organoid
811 Growth Medium (Mouse) (#06005 STEMCELL) supplemented with 1% Pen/Strep (Gibco 15140).
812 After isolation, the organoids were maintained for two passages by resuspending them in cold
813 media mixed with Matrigel (Fisher Scientific CB40230C) at a 1:1 ratio. In each passage, five 40 µL
814 droplets of the cell suspension were plated in a 6-well plate, incubated at 37°C for 20 minutes, and
815 then 3 mL of pre-warmed media was added. AKP and metastatic organoids were cultured in ADF+
816 media, composed of Advanced DMEM F12 (Invitrogen) supplemented with 5% heat-inactivated
817 FBS (Sigma-Aldrich), 1% Penicillin-Streptomycin-Glutamine (Invitrogen), and 1% HEPES
818 (Invitrogen). These organoids were plated in droplets, following the same procedure as for the
819 mouse-derived organoid passages. To prepare the cells for lysis, all organoids were dissociated in
820 cold ADF+ media to break down the Matrigel. The cell suspensions were centrifuged at 1000 rpm
821 for 5 minutes. After removing the supernatant, 1 mL of TrypLE (Thermo Fisher Scientific
822 12605010) was added to the cell pellet, followed by incubation in a 37°C water bath for 25
823 minutes. To stop the dissociation and wash the cells, 5 mL of ADF+ media was added to each
824 organoid type. Cells were then pelleted again by centrifugation at 1500 rpm, and the supernatant
825 was carefully removed. For the pulldown, cells were lysed using a lysis buffer consisting of 0.50%
826 Igepal CA-630 in 1x PBS supplemented with a protease inhibitor cocktail (Roche). The cell pellet
827 was resuspended in 500 µL of this lysis buffer and briefly vortexed. The lysate was incubated on
828 ice for 30 minutes to ensure complete lysis and then centrifuged at 14,000 g for 10 minutes at 4°C.
829 Meanwhile, Pierce™ Protein L Magnetic Beads (Thermo Scientific) were washed by adding 100 µL
830 of beads to 300 µL of PBS-T in six tubes. The beads were gently vortexed for 1 minute and
831 collected using a magnet. After removing the supernatant, the beads were washed again with 1 mL
832 of PBS-T, followed by gentle vortexing and removal of the supernatant. The resulting lysis
833 supernatant of each organoid was transferred to two different tubes containing the washed beads
834 - 240 µL of supernatant added to each tube. The division was made to achieve two conditions: one
835 that received the faecal SIgA and one negative control, where the supernatant was incubated with
836 beads in the absence of SIgA. Next, 100 µL of SIgA (at a concentration of 600 µg/mL) was
837 introduced into each designated tube, and the positive and negative mixtures were incubated for 2
838 hours at 4°C with gentle agitation. The beads were then collected using a magnet, and the
839 supernatant was removed. The beads were washed three times with 200 µL of PBS-T, vortexed
840 briefly and carefully between washes, and collected using a magnet to remove the supernatant

841 each time. Finally, 22.5 μL of elution buffer (0.1M glycine at pH 2-2.5) was added to the beads, and
842 the mixture was incubated at room temperature for 10 minutes with occasional vortexing. The
843 eluate was combined with 2.5 μL of 1M Tris-HCl at pH 8. Proteins bound to magnetic beads were
844 eluted through partial trypsin digestion (Promega). The supernatants were reduced with DTT,
845 alkylated using iodoacetamide, and subjected to overnight redigestion with trypsin and
846 Endopeptidase LysC (Wako/Fuji). Digestion was halted with TFA, followed by peptide cleanup via
847 solid-phase extraction (SPE'ed). The peptides were then analyzed by LC-MS/MS, utilizing a 70-
848 minute analytical gradient (2%B to 38%B) on a 12 cm built-in emitter column with high
849 resolution and mass accuracy (EasyLC1200 and Lumos Fusion, Thermo Fisher). The resulting data
850 was searched against the UniProt mouse database, concatenated with common contaminants,
851 using Proteome Discoverer (v1.4.1.14) and MASCOT (v2.8.01). Data were filtered with a
852 Percolator-calculated false discovery rate (FDR) of 1% or better. Further processing was done by
853 filtering peptide-spectrum match (PSM) counts for each protein and organizing them into a count
854 matrix. Missing values were imputed as zero. The matrix was used to generate a DESeq2 object,
855 and results were obtained without fold change (FC) shrinkage. Differential analysis was
856 performed to identify significant changes in protein abundance between IgA+ and IgA- groups.
857 Results were visualized using a volcano plot, where proteins with Log2FC ≥ 1 or ≤ -1 and adjusted
858 p-values < 0.05 were considered for downstream analysis.
859
860 Statistical methods
861 Unless otherwise state, mean and standard error are plotted for all figures. For comparisons
862 between two groups, two-tailed unpaired t-tests were performed. For three or more groups,
863 ordinary one-way ANOVA tests were performed with Dunnett's correction for multiple
864 comparisons. Exact p values are reported on graphs when the p value or adjusted p value is less
865 than 0.1. For sequencing analyses, application-specific statistical methods are described in the
866 respective methods sections or figure legends.
867
868 **Data Availability**
869 All raw sequencing data for bulk RNA-Seq, 16S rRNA amplicon sequencing, and single cell RNA-
870 Seq are available on the NCBI Sequence Read Archive (SRA) under a unified project:
871 PRJNA1023250.

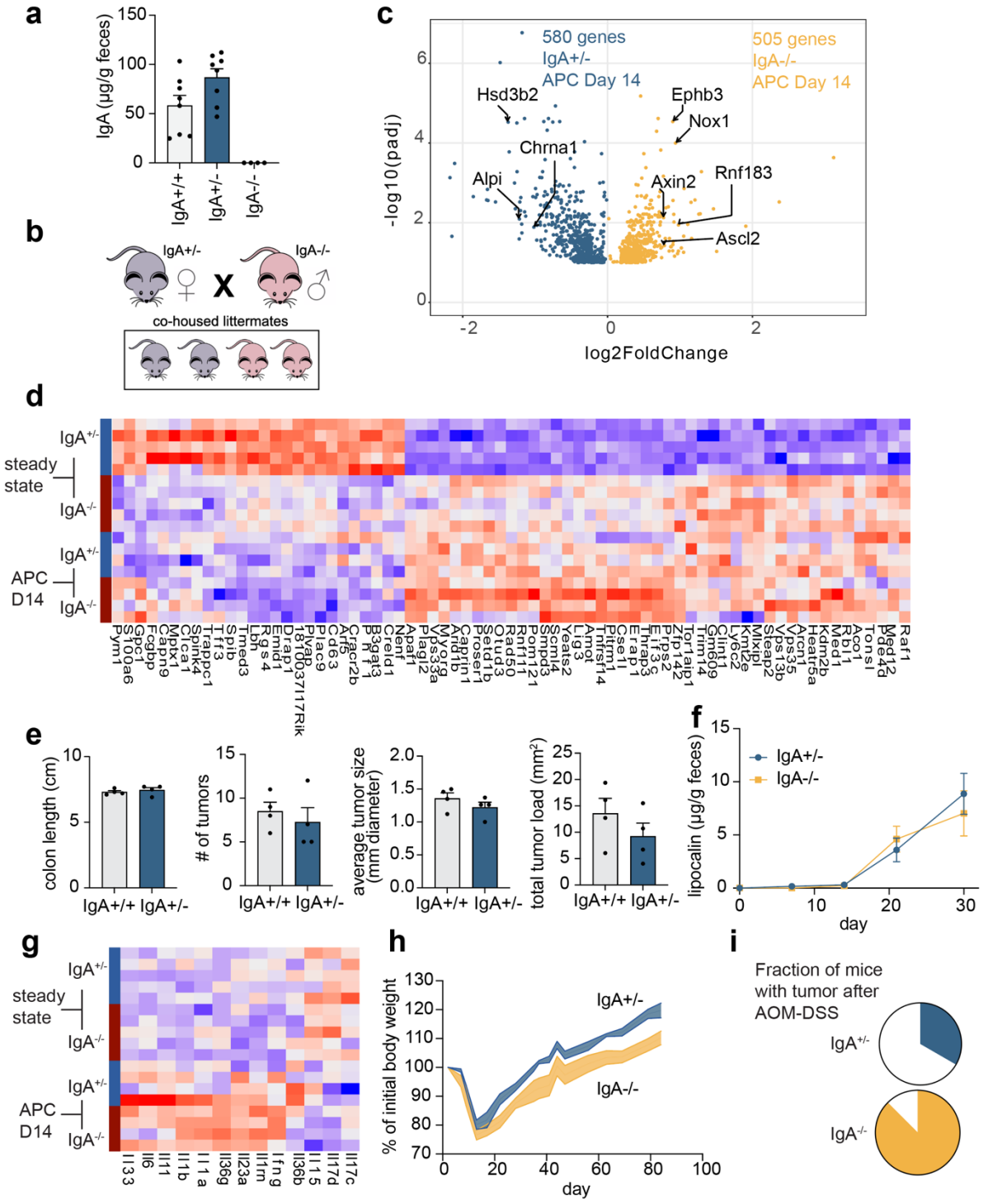

Extended Data Fig. 1 | Additional data related to Fig. 1. a, ELISA of faecal IgA in homozygotes and heterozygotes of the IgA$^{-/-}$ strain crossed with C57BL6/J (n = 8, 8, 4). **b**, Breeding scheme for littermate controls. **c**, Differentially expressed genes in bulk RNA-Seq from mid-colon tissue of IgA$^{+/-}$ and IgA$^{-/-}$ littermates fourteen days after inducing colon epithelial-specific loss of *APC* (n = 4). **d**, Set of genes identified as modulated by both *APC* loss (steady state vs. APC Day 14 comparison) and IgA deficiency at steady state (IgA$^{+/-}$ vs. IgA$^{-/-}$). Interestingly, the direction of the effect of IgA deficiency is toward the direction caused by *APC* loss (n = 5, 5, 4, 4). **e**, Endpoint

881 analyses of the APC-driven cancer model using $IgA^{+/+}$ and $IgA^{+/-}$ littermates (n = 4). **f**, ELISA for
882 faecal lipocalin in the APC-driven cancer model (n = 3, from one cohort, representative). **g**,
883 Cytokine gene expression in the bulk colon tissue RNA-Seq shows no IgA-dependent alterations in
884 inflammatory pathways (n = 5, 5, 4, 4). **h**, Body weight change during AOM-DSS (n = 4, from one
885 cohort, representative). **i**, Tumour frequency in the AOM-DSS cancer model (n = 9, 8).

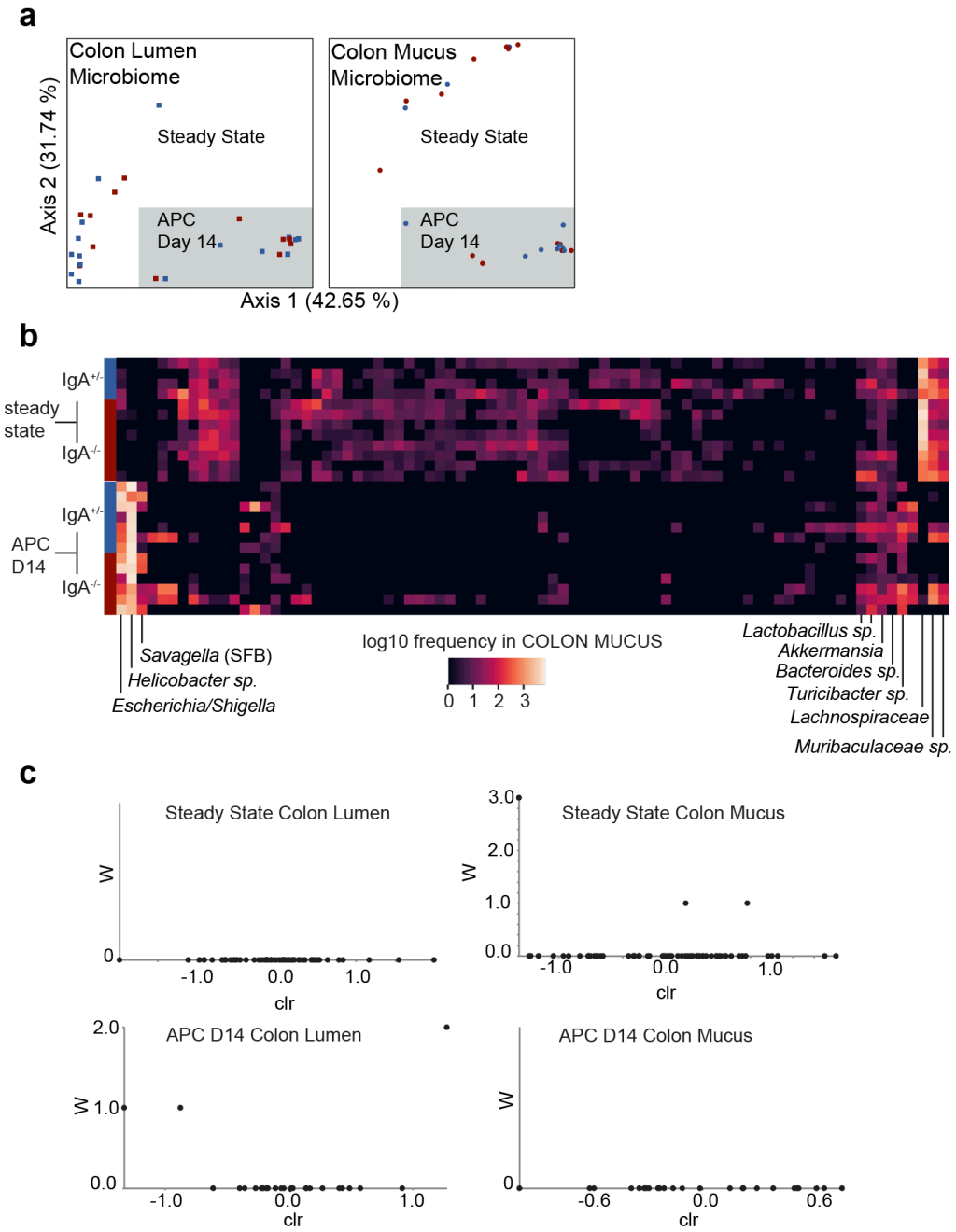

Extended Data Fig. 2 | Additional microbiome profiling data. a, Beta diversity (weighted unifrac distance) of microbiome measured by 16S rRNA amplicon sequencing of samples from IgA$^{+/-}$ (blue) and IgA$^{-/-}$ (red) mice showing no genotype-specific alterations (lumen n = 9, 6, 7, 6, mucus n = 4, 8, 7, 6). **b**, Heatmap of amplicon sequence variants (columns) identified in colon mucus samples from indicated mice (rows) demonstrates dramatic shift caused by *APC* loss, but no effect of IgA. **c**, ANCOM differential abundance testing of IgA$^{+/-}$ vs. IgA$^{-/-}$ littermates in the indicated sample types identified no IgA-dependent alterations in the microbiome.

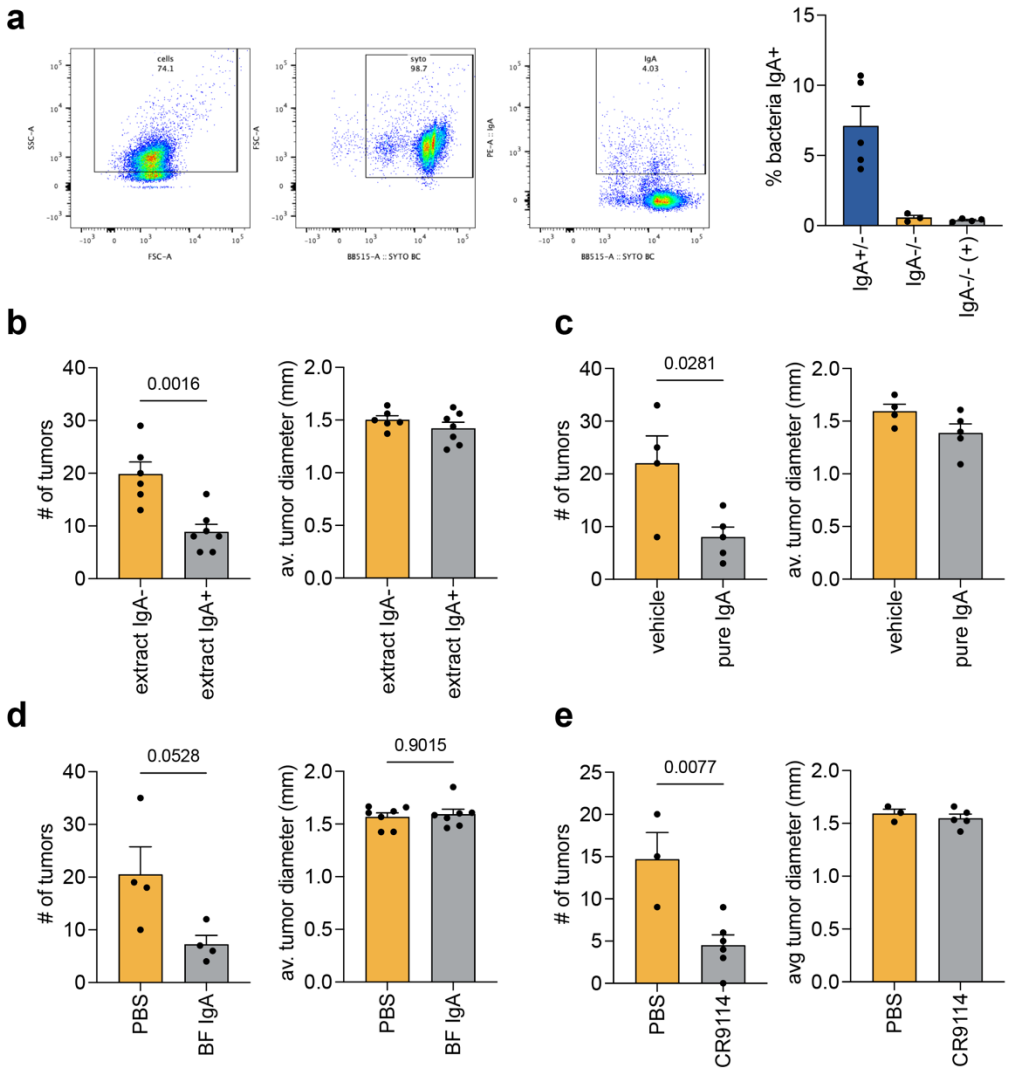

Extended Data Fig. 3 | Additional results related to IgA gavage treatments. a, Gating strategy for flow cytometry for IgA coating of bacterial cells in faecal samples and summary data showing a lack of IgA binding to bacteria when IgA$^{-/-}$ mice were gavaged with faecal IgA purified from germfree mice monocolonized with *Bacteroides fragilis* (n = 5, 3, 4). **b-e**, Counts and sizes of tumours from IgA$^{-/-}$ mice treated with **b**, faecal extracts (n = 6, 7), **c**, purified faecal IgA from SPF mice (n = 4, 5), **d**, purified faecal IgA from mice mono-colonized with *Bacteroides fragilis* (n = 4), or **e**, recombinant CR9114 anti-influenza HA monoclonal secretory IgA (n = 3, 5).

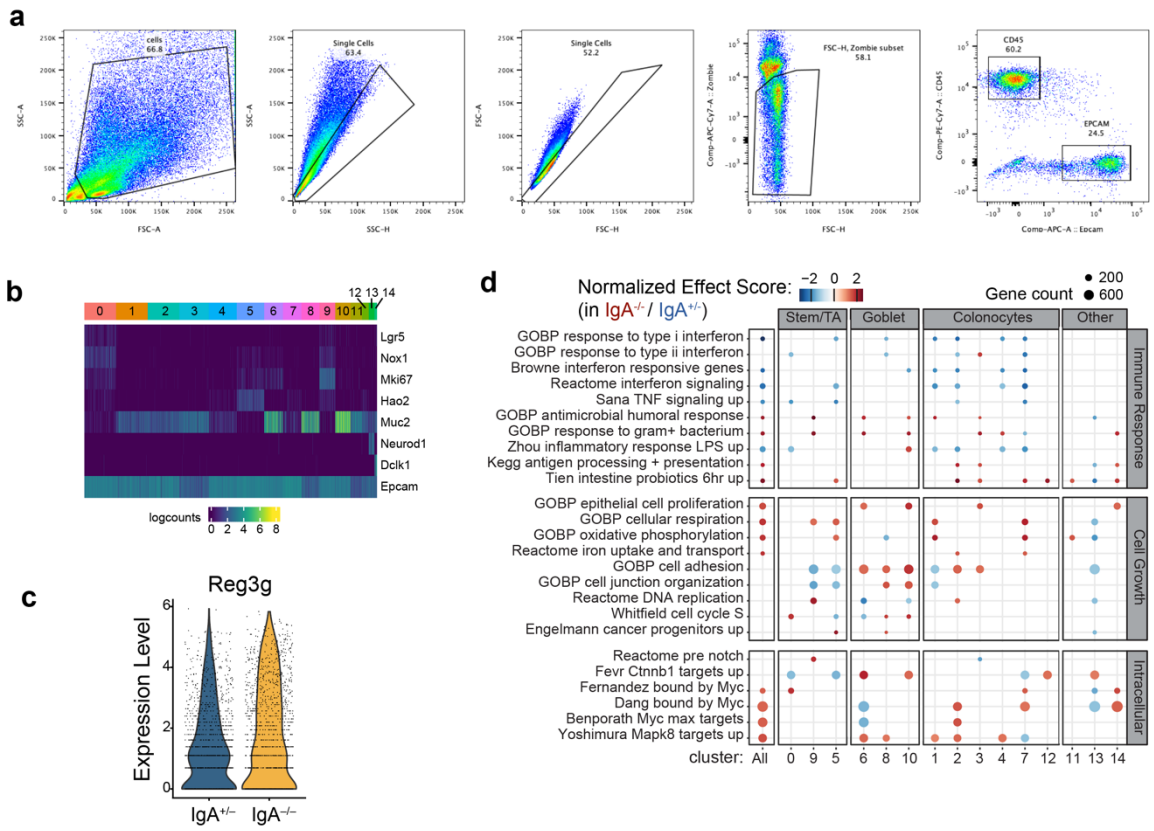

Extended Data Fig. 4 | Additional data related to colon epithelial single cell RNA-Seq. a, Gating strategy for sorting live EPCAM+, CD45- epithelial cells for single-cell transcriptomics (n = 3). **b**, Various markers to aid in identifying clusters: *Lgr5* (stem), *Nox1* (transit-amplifying), *Mki67* (cycling), *Hao2* (immature), *Muc2* (low: mature, high: goblet), *Neurod1* (enteroendocrine), *Dclk1* (Tuft), and *Epcam* (pan-epithelial). **c**, Expression level of the antimicrobial *Reg3g* in all cells. **d**, Full version of Fig. 3g with all clusters: Gene set enrichment analyses in individual clusters based on IgA genotype. Dots are visible where adjusted p value < 0.05, size of dot represents the number of genes int he pathway, and color represents the normalized enrichment score of that pathway ($IgA^{-/-}$-enriched is positive, red).

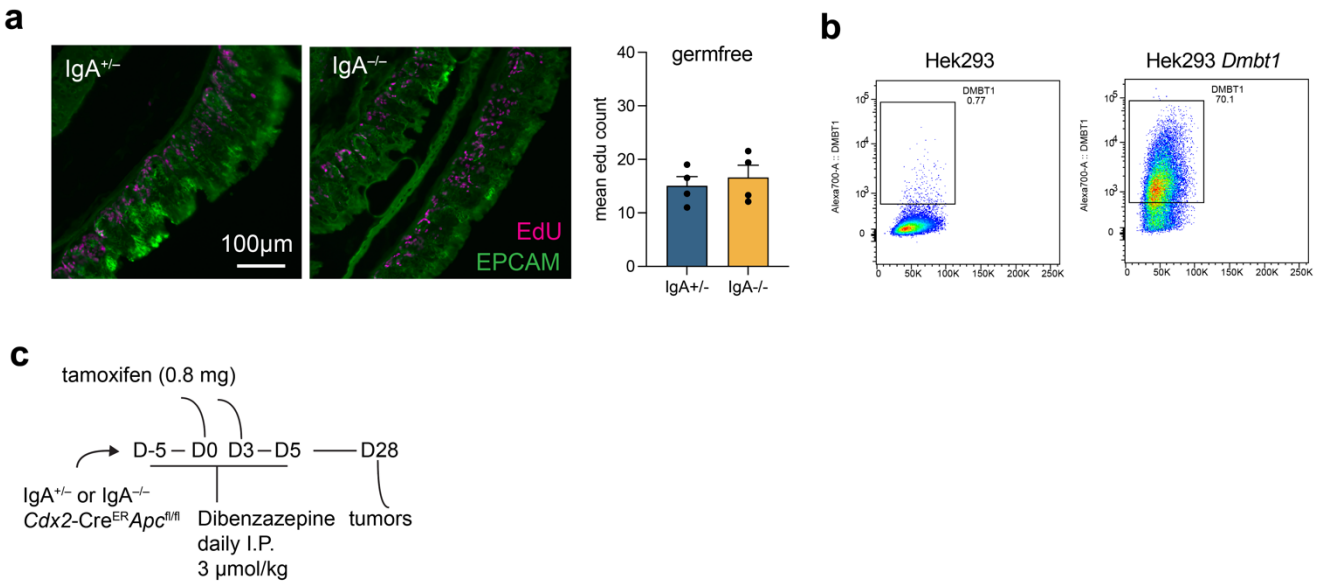

Extended Data Fig. 5 | Additional data related to epithelial proliferation. a, EdU (pink) and EPCAM (green) staining in germfree mice after two injections (-24 hours and -4 hours) of EdU showed no difference between IgA$^{+/-}$ and IgA$^{-/-}$ littermates (n = 4). **b**, Flow cytometry of surface DMBT1 on HEK293 cells: wildtype (left) and expressing a membrane isoform of *Dmbt1* (right). **c**, Experimental design for Notch inhibition to suppress epithelial proliferation in the context of IgA deficiency and *APC* loss.

927 **References**

928

929 1. Fagarasan, S. Evolution, development, mechanism and function of IgA in the gut. *Curr. Opin.*
930 *Immunol.* **20**, 170–177 (2008).

931 2. Pabst, O. & Slack, E. IgA and the intestinal microbiota: the importance of being specific. *Mucosal*
932 *Immunol.* **13**, 12–21 (2020).

933 3. Huus, K. E., Petersen, C. & Finlay, B. B. Diversity and dynamism of IgA–microbiota interactions. *Nat*
934 *Rev Immunol* 1–12 (2021) doi:10.1038/s41577-021-00506-1.

935 4. Catanzaro, J. R. *et al.* IgA-deficient humans exhibit gut microbiota dysbiosis despite secretion of
936 compensatory IgM. *Scientific reports* **9**, 13574–10 (2019).

937 5. Yel, L. Selective IgA deficiency. *Journal of clinical immunology* (2010) doi:10.1007/s10875-009-
938 9357-x.

939 6. Fadlallah, J. *et al.* Microbial ecology perturbation in human IgA deficiency. *Science Translational*
940 *Medicine* **10**, eaan1217 (2018).

941 7. Conrey, P. E. *et al.* IgA deficiency destabilizes homeostasis toward intestinal microbes and increases
942 systemic immune dysregulation. *Sci Immunol* **8**, eade2335 (2023).

943 8. Moll, J. M. *et al.* Gut microbiota perturbation in IgA deficiency is influenced by IgA-autoantibody
944 status. *Gastroenterology* (2021) doi:10.1053/j.gastro.2021.02.053.

945 9. Shroff, K. E., Meslin, K. & Cebra, J. J. Commensal enteric bacteria engender a self-limiting humoral
946 mucosal immune response while permanently colonizing the gut. *Infection and immunity* **63**, 3904–
947 3913 (1995).

948 10. Singh, K., Chang, C. & Gershwin, M. E. IgA deficiency and autoimmunity. *Autoimmunity reviews* **13**,
949 163–177 (2014).

950 11. Ludvigsson, J. F., Neovius, M., Ye, W. & Hammarström, L. IgA deficiency and risk of cancer: a
951 population-based matched cohort study. *Journal of clinical immunology* **35**, 182–188 (2015).

952 12. Langford, T. D. *et al.* Central Importance of Immunoglobulin A in Host Defense against Giardia spp.
953 *Infect Immun* **70**, 11–18 (2002).

954 13. Blutt, S. E., Miller, A. D., Salmon, S. L., Metzger, D. W. & Conner, M. E. IgA is important for clearance
955 and critical for protection from rotavirus infection. *Mucosal immunology* **5**, 712–719 (2012).

956 14. Moor, K. *et al.* High-avidity IgA protects the intestine by enchaining growing bacteria. *Nature* **544**,
957 498–502 (2017).

958 15. Jørgensen, S. F. *et al.* Selective IgA deficiency in humans is associated with reduced gut microbial
959 diversity. *The Journal of allergy and clinical immunology* **143**, 1969-1971.e11 (2019).

960 16. Gatti, R. A. & Good, R. A. Occurrence of malignancy in immunodeficiency diseases: A literature
961 review. *Cancer* **28**, 89–98 (1971).

962 17. Filipovich, A. H., Mathur, A., Kamat, D., Kersey, J. H. & Shapiro, R. S. Lymphoproliferative disorders
963 and other tumors complicating immunodeficiencies. *Immunodefic* **5**, 91–112 (1994).

964 18. Tjalsma, H., Boleij, A., Marchesi, J. R. & Dutilh, B. E. A bacterial driver–passenger model for
965 colorectal cancer: beyond the usual suspects. *Nat Rev Microbiol* **10**, 575–582 (2012).

966 19. Cullin, N., Antunes, C. A., Straussman, R., Stein-Thoeringer, C. K. & Elinav, E. Microbiome and cancer.
967 *Cancer Cell* (2021) doi:10.1016/j.ccell.2021.08.006.

968 20. Clay, S. L., Fonseca-Pereira, D. & Garrett, W. S. Colorectal cancer: the facts in the case of the
969 microbiota. *J Clin Invest* **132**, e155101 (2022).

970 21. Ludvigsson, J. F., Neovius, M. & Hammarström, L. IgA Deficiency & Mortality: A Population-Based
971 Cohort Study. *J Clin Immunol* **33**, 1317–1324 (2013).

972 22. Cunningham-Rundles, C., Pudifin, D. J., Armstrong, D. & Good, R. A. Selective IgA Deficiency and
973 Neoplasia. *Vox Sang* **38**, 61–67 (1980).

974 23. Pulvirenti, F. *et al.* Gastric Cancer Is the Leading Cause of Death in Italian Adult Patients With
975 Common Variable Immunodeficiency. *Front Immunol* **9**, 2546 (2018).

976 24. Shulzhenko, N. *et al.* Crosstalk between B lymphocytes, microbiota and the intestinal epithelium
977 governs immunity versus metabolism in the gut. *Nature medicine* **17**, 1585–1593 (2011).

978 25. Kawamoto, S. *et al.* The inhibitory receptor PD-1 regulates IgA selection and bacterial composition
979 in the gut. *Science* **336**, 485–489 (2012).

980 26. Kubinak, J. L. *et al.* MyD88 signaling in T cells directs IgA-mediated control of the microbiota to
981 promote health. *Cell host & microbe* **17**, 153–163 (2015).

982 27. Suzuki, K. *et al.* Aberrant expansion of segmented filamentous bacteria in IgA-deficient gut.
983 *Proceedings of the National Academy of Sciences of the United States of America* **101**, 1981–1986
984 (2004).

985 28. Fagarasan, S. *et al.* Critical roles of activation-induced cytidine deaminase in the homeostasis of gut
986 flora. *Science* **298**, 1424–1427 (2002).

987 29. Gopalakrishna, K. P. *et al.* Maternal IgA protects against the development of necrotizing
988 enterocolitis in preterm infants. *Nat Med* **25**, 1110–1115 (2019).

989 30. Kawamoto, S. *et al.* Foxp3(+) T cells regulate immunoglobulin a selection and facilitate
990 diversification of bacterial species responsible for immune homeostasis. *Immunity* **41**, 152–165
991 (2014).

992 31. Nagashima, K. *et al.* Identification of subepithelial mesenchymal cells that induce IgA and diversify
993 gut microbiota. *Nat Immunol* **18**, 675–682 (2017).

994 32. Bunker, J. J. *et al.* Natural polyreactive IgA antibodies coat the intestinal microbiota. *Science* **358**,
995 eaan6619 (2017).

996 33. Shimoda, M., Inoue, Y., Azuma, N. & Kanno, C. Natural polyreactive immunoglobulin A antibodies
997 produced in mouse Peyer's patches. *Immunity* **97**, 9–17 (1999).

998 34. Rollenske, T. *et al.* Cross-specificity of protective human antibodies against Klebsiella pneumoniae
999 LPS O-antigen. *Nature immunology* **19**, 617–624 (2018).

000 35. Kabbert, J. *et al.* High microbiota reactivity of adult human intestinal IgA requires somatic
001 mutations. *The Journal of experimental medicine* **217**, (2020).

002 36. Nowosad, C. R. *et al.* Tunable dynamics of B cell selection in gut germinal centres. *Nature* **588**, 321–
003 326 (2020).

004 37. Peterson, D. A. *et al.* Characterizing the Interactions Between a Naturally-primed Immunoglobulin
005 A and its Conserved Bacteroides thetaiotaomicron Species-specific Epitope in Gnotobiotic Mice. *The*
006 *Journal of biological chemistry* (2015) doi:10.1074/jbc.m114.633800.

007 38. Nakajima, A. *et al.* IgA regulates the composition and metabolic function of gut microbiota by
008 promoting symbiosis between bacteria. *The Journal of experimental medicine* **67**, jem.20180427-2034
009 (2018).

010 39. Donaldson, G. P. *et al.* Gut microbiota utilize immunoglobulin A for mucosal colonization. *Science*
011 **360**, 795–800 (2018).

012 40. Rollenske, T. *et al.* Parallelism of intestinal secretory IgA shapes functional microbial fitness.
013 *Nature* 1–5 (2021) doi:10.1038/s41586-021-03973-7.

014 41. Harriman, G. R. *et al.* Targeted deletion of the IgA constant region in mice leads to IgA deficiency
015 with alterations in expression of other Ig isotypes. *The Journal of Immunology* **162**, 2521–2529 (1999).

016 42. Murthy, A. K., Dubose, C. N., Banas, J. A., Coalson, J. J. & Arulanandam, B. P. Contribution of
017 polymeric immunoglobulin receptor to regulation of intestinal inflammation in dextran sulfate
018 sodium-induced colitis. *Journal of gastroenterology and hepatology* **21**, 1372–1380 (2006).

019 43. Mathias, A. & Corthésy, B. N-Glycans on secretory component: mediators of the interaction
020 between secretory IgA and gram-positive commensals sustaining intestinal homeostasis. *Gut microbes*
021 **2**, 287–293 (2011).

022 44. Kaetzel, C. S. The polymeric immunoglobulin receptor: bridging innate and adaptive immune
023 responses at mucosal surfaces. *Immunol. Rev.* **206**, 83–99 (2005).

024 45. Ramanan, D. *et al.* An Immunologic Mode of Multigenerational Transmission Governs a Gut Treg
025 Setpoint. *Cell* **181**, 1276-1290.e13 (2020).

026 46. Robertson, S. J. *et al.* Comparison of Co-housing and Littermate Methods for Microbiota
027 Standardization in Mouse Models. *Cell Rep.* **27**, 1910-1919.e2 (2019).

028 47. Donaldson, G. P., Lee, S. M. & Mazmanian, S. K. Gut biogeography of the bacterial microbiota. *Nature*
029 *reviews. Microbiology* **14**, 20–32 (2015).

030 48. Post, S. van der, Birchenough, G. M. H. & Held, J. M. NOX1-dependent redox signaling potentiates
031 colonic stem cell proliferation to adapt to the intestinal microbiota by linking EGFR and TLR activation.
032 *Cell Reports* **35**, 108949 (2021).

033 49. Grivennikov, S. I. *et al.* Adenoma-linked barrier defects and microbial products drive IL-23/IL-17-
034 mediated tumour growth. *Nature* **491**, 254–258 (2012).

035 50. Grivennikov, S. I. Inflammation and colorectal cancer: colitis-associated neoplasia. *Seminars in*
036 *immunopathology* **35**, 229–244 (2013).

037 51. Mandal, S. *et al.* Analysis of composition of microbiomes: a novel method for studying microbial
038 composition. *Microb. Ecol. Heal. Dis.* **26**, 27663 (2015).

039 52. Brugiroux, S. *et al.* Genome-guided design of a defined mouse microbiota that confers colonization
040 resistance against Salmonella enterica serovar Typhimurium. *Nature microbiology* **2**, 16215 (2016).

041 53. Beumer, J. & Clevers, H. Cell fate specification and differentiation in the adult mammalian intestine.
042 *Nat. Rev. Mol. Cell Biol.* **22**, 39–53 (2021).

043 54. Tsang, D. K. L. *et al.* A single cell survey of the microbial impacts on the mouse small intestinal
044 epithelium. *Gut Microbes* **14**, 2108281 (2022).

045 55. Rakoff-Nahoum, S., Paglino, J., Eslami-Varzaneh, F., Edberg, S. & Medzhitov, R. Recognition of
046 Commensal Microflora by Toll-Like Receptors Is Required for Intestinal Homeostasis. *Cell* **118**, 229–
047 241 (2004).

048 56. Sato, T. *et al.* Single Lgr5 stem cells build crypt-villus structures in vitro without a mesenchymal
049 niche. *Nature* **459**, 262–265 (2009).

050 57. Merenda, A., Fenderico, N. & Maurice, M. M. Wnt Signaling in 3D: Recent Advances in the
051 Applications of Intestinal Organoids. *Trends Cell Biol.* **30**, 60–73 (2020).

052 58. Rundegren, J. & Arnold, R. R. Differentiation and interaction of secretory immunoglobulin A and a
053 calcium-dependent parotid agglutinin for several bacterial strains. *Infect. Immun.* **55**, 288–292 (1987).

054 59. Mollenhauer, J. *et al.* The genomic structure of the DMBT1 gene: evidence for a region with
055 susceptibility to genomic instability. *Oncogene* **18**, 6233–6240 (1999).

056 60. Fre, S. *et al.* Notch signals control the fate of immature progenitor cells in the intestine. *Nature* **435**,
057 964–968 (2005).

058 61. Es, J. H. van *et al.* Notch/γ-secretase inhibition turns proliferative cells in intestinal crypts and
059 adenomas into goblet cells. *Nature* **435**, 959–963 (2005).

060 62. Biswas, S. *et al.* IgA transcytosis and antigen recognition govern ovarian cancer immunity. *Nature*
061 **591**, 464–470 (2021).

062 63. Pelka, K. *et al.* Spatially organized multicellular immune hubs in human colorectal cancer. *Cell* **184**,
063 4734-4752.e20 (2021).

064 64. Chalkias, A. *et al.* Patients with colorectal cancer are characterized by increased concentration of
065 fecal hb-hp complex, myeloperoxidase, and secretory IgA. *American Journal of Clinical Oncology* **34**,
066 561–566 (2011).

067 65. Tang, Y. *et al.* MZB1-mediated IgA secretion suppresses the development and progression of
068 colorectal cancer triggered by gut inflammation. *Mucosal Immunol.* (2023)
069 doi:10.1016/j.mucimm.2023.12.002.

070 66. Pleguezuelos-Manzano, C. *et al.* Mutational signature in colorectal cancer caused by genotoxic
071 pks+E. coli. *Nature* **580**, 269–273 (2020).

072 67. Kabatnik, S. *et al.* Spatial characterization and stratification of colorectal adenomas by Deep Visual
073 Proteomics. *medRxiv* 2023.11.25.23298987 (2023) doi:10.1101/2023.11.25.23298987.

074 68. Park, H. S. *et al.* Deleted in malignant brain tumor 1 is a novel prognostic marker in colorectal
075 cancer. *Oncol. Rep.* **39**, 2279–2287 (2018).

076 69. Du, J., Guan, M., Fan, J. & Jiang, H. Loss of DMBT1 Expression in Human Prostate Cancer and Its
077 Correlation with Clinical Progressive Features. *Urology* **77**, 509.e9-509.e13 (2011).

078 70. Rosenstiel, P. *et al.* Regulation of DMBT1 via NOD2 and TLR4 in Intestinal Epithelial Cells
079 Modulates Bacterial Recognition and Invasion. *J. Immunol.* **178**, 8203–8211 (2007).

080 71. Fuess, L. E., C., J. H. P., Weil, E. & Mydlarz, L. D. Associations between transcriptional changes and
081 protein phenotypes provide insights into immune regulation in corals. *Dev. Comp. Immunol.* **62**, 17–28
082 (2016).

083 72. Müller, H. *et al.* Deleted in Malignant Brain Tumors 1 is Present in the Vascular Extracellular Matrix
084 and Promotes Angiogenesis. *Arter., Thromb., Vasc. Biol.* **32**, 442–448 (2012).

085 73. Hopkins, E. G. D., Roumeliotis, T. I., Mullineaux-Sanders, C., Choudhary, J. S. & Frankel, G. Intestinal
086 Epithelial Cells and the Microbiome Undergo Swift Reprogramming at the Inception of Colonic
087 Citrobacter rodentium Infection. *mBio* **10**, e00062-19 (2019).

088 74. Renner, M. *et al.* DMBT1 Confers Mucosal Protection In Vivo and a Deletion Variant Is Associated
089 With Crohn's Disease. *Gastroenterology* **133**, 1499–1509 (2007).

090 75. Reikvam, D. H., Derrien, M. & Islam, R. Epithelial-microbial crosstalk in polymeric Ig receptor
091 deficient mice. *European journal of …* (2012) doi:10.1002/eji.201242543.

092 76. Tsuruta, T. *et al.* The amount of secreted IgA may not determine the secretory IgA coating ratio of
093 gastrointestinal bacteria. *Fems Immunol Medical Microbiol* **56**, 185–189 (2009).

094 77. Burrows, P. D. & Cooper, M. D. IgA Deficiency. *Advances in Immunology*.

095 78. Dmitrieva-Posocco, O. *et al.* β-Hydroxybutyrate suppresses colorectal cancer. *Nature* **605**, 160–165
096 (2022).

097 79. Earley, Z. M. *et al.* GATA4 controls regionalization of tissue immunity and commensal-driven
098 immunopathology. *Immunity* **56**, 43-57.e10 (2023).

099 80. Bharathkar, S. K. *et al.* The structures of secretory and dimeric immunoglobulin A. *Elife* **9**, e56098
100 (2020).

101 81. Dreyfus, C. *et al.* Highly Conserved Protective Epitopes on Influenza B Viruses. *Science* **337**, 1343–
102 1348 (2012).

103 82. Miyoshi, H. & Stappenbeck, T. S. In vitro expansion and genetic modification of gastrointestinal
104 stem cells in spheroid culture. *Nat. Protoc.* **8**, 2471–2482 (2013).

105 83. Sanjana, N. E., Shalem, O. & Zhang, F. Improved vectors and genome-wide libraries for CRISPR
106 screening. *Nat. Methods* **11**, 783–784 (2014).

107 84. Roper, J. *et al.* In vivo genome editing and organoid transplantation models of colorectal cancer and
108 metastasis. *Nat. Biotechnol.* **35**, 569–576 (2017).

109